




Review Paper

A review: advancements in fluoro-based polymers for aggrandizing anti-galling and wear resistant characteristics



Kalpesh K. Kakulite¹ · Shivpal Singh Panwar² · Balasubramanian Kandasubramanian¹ 

© Springer Nature Switzerland AG 2019

Abstract

Galling is the surface phenomenon which involves adhesion of local contact points and creation of protrusions on the juxtaposition of surfaces owing to high friction, inappropriate tribological loading, starved lubrication and high contact pressure (~ 1000 kPa). All these factors result in severe plastic deformation varying from 8000 to 10,000 $\mu\epsilon$ (ϵ -strain) and diffusion of materials into one another, which consequently results in fatigue wear, surface roughness, tribocorrosion and seizing up of critical parts. The aim of the review is to analyze and summarize the issue of galling, concurrently it also deals with the novel and economical mitigation method i.e. use of fluorine based coatings e.g. PTFE, owing to their lowest friction coefficient from 0.02 to 0.2 among other solids, high stiffness, high thermal stability and non-adherent characteristics that augments the mechanical and tribological properties and concurrently protect against hostile environments that eventually upsurgences the life of components.

✉ Balasubramanian Kandasubramanian, meetkbs@gmail.com | ¹Structural Composite Fabrication Laboratory, Department of Metallurgical and Materials Engineering, Defence Institute of Advanced Technology (DU), Ministry of Defence, Girinagar, Pune, Maharashtra 411025, India. ²Defence Research and Development Laboratory (DRDL), Defence Research and Development Organization, Hyderabad, Telangana 500005, India.

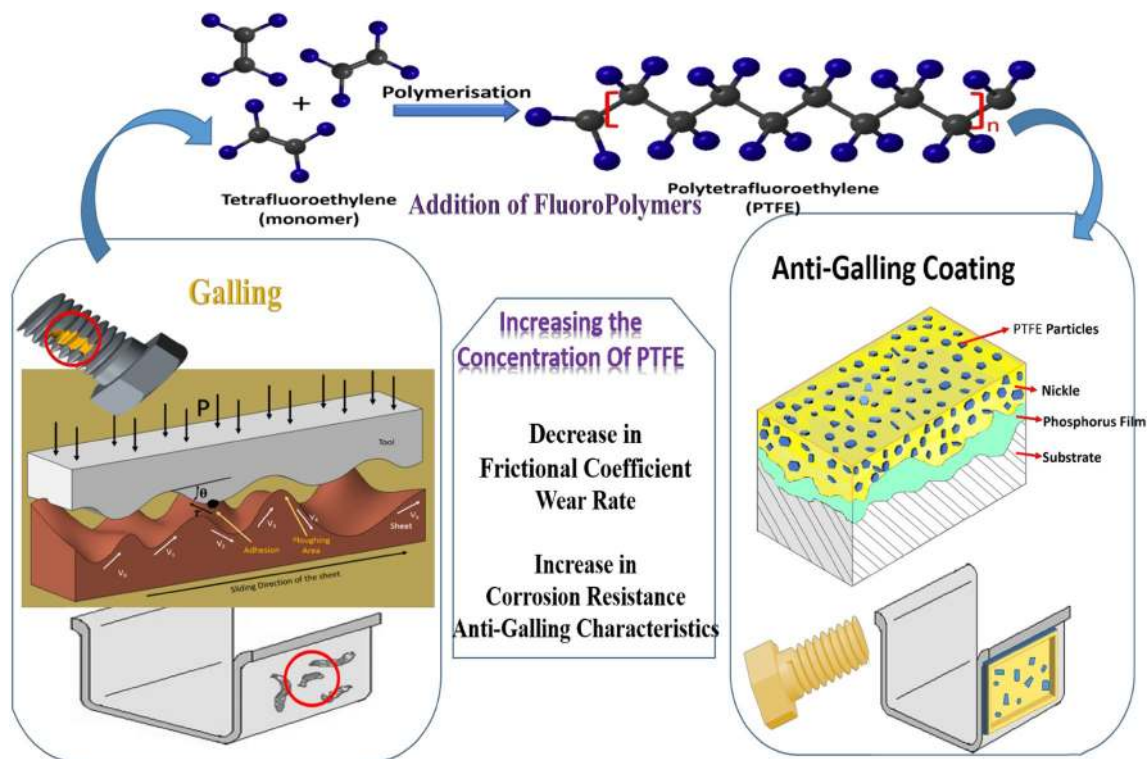


SN Applied Sciences (2019) 1:942 | <https://doi.org/10.1007/s42452-019-0924-3>

Received: 27 March 2019 / Accepted: 12 July 2019 / Published online: 30 July 2019

SN Applied Sciences
A SPRINGER NATURE journal

Graphic Abstract



Keywords Fluoro · Coating · Galling · Tribological · PTFE

List of symbols

F_R	Force of friction (N)	d	Distance moved (m)
F_N	Applied normal force (N)	FCC	Face centered cubic structure
μ	Coefficient of friction	HCP	Hexagonal cubic packed structure
σ	Stress applied (N/m ²)		
A	Contact area (M)		
E	Youngs modulus (Mpa)		
ψ	Plasticity index		
q	Heat generation during sliding (W)		
V	Velocity of sliding (m/s)		
HV	Hardness value		
R_s	Radius of contact (m)		
T_F	Flash temperature (°C)		
K_{eff}	Effective thermal coefficient (W/mK)		
a, b	Axis length of ellipse (M)		
T_{cr}	Critical temperature (°C)		
α_s	Thermal diffusivity (m ² /s)		
W_{sep}	Work of separation (Nm)		
$E_{interface}$	Total energy of system (Nm)		
$E_{Fe-fixed}$	Total energy possessed by the disengaged slab of Fe (Nm)		
$E_{TiC-fixed}$	Total energy possessed by the disengaged slab of TiC (Nm)		
T_y	Torque applied (Nm)		

1 Introduction

From the evolution of mankind, humans had intuitively started to scrutinize the rudimentary characteristics of materials in order to complete their day-to-day activities, i.e. from selection of glossy beads used to make bracelets to the selection of a hard material for making tools such as axe and hammer chisel [1] or the invention of fire due to surface friction owing to rubbing of stones [2, 3] or scrubbing of proper wood in fine sawdust form [4, 5]. Although every mechanical device is upgrading itself in the fast-paced advanced technology, it is inevitable to manufacture products without inherent surface defects like roughness and waviness resulting in the variation of contact conditions during mating of surfaces and has become a foremost task for researchers to encounter all this issues without compromising performance of the system [6, 7]. Now, without having considerable background of research in the behavior of sliding surfaces, it will be

challenging to achieve precision and reliability required for various engineering components. Friction has merits and flaws, it can result in the stability of wheels during motion at the same moment it can result in wear down of the same wheel due to frictional heat. Leonardo da Vinci, Euler and A. Coulomb consistently and arithmetically framed the basic laws of friction and arrived at the outcome that can be summarized in today's language as two fundamental Laws of Friction.

First, the force of friction is proportional to the normal force (load) applied on a body.

$$F_R = \mu F_N \quad (1)$$

where ' F_R ' is the force of friction, ' F_N ' is the external force (s) applied on the body, and ' μ ' denotes the 'coefficient of friction' between the sliding surfaces.

Second, the force of friction is independent of the contact surface area [7–9].

Then after many researchers used these fundamentals of friction to analyze the eventualities occurred due to friction such as heat generation, wear and galling during the mating, rubbing and sliding of surfaces over each other and categorize as "Tribology" by Peter Jost in the year 1966. Tribology is a term that covers the concepts of chemistry, physics, fluid mechanics, heat transfer, solid mechanics, material science, lubricant rheology, reliability, and performance of the mating surfaces [9].

Primarily researchers tried to interlace the fundamentals of friction with the contacted surface area during sliding as depicted in Fig. 1. The apparent contact area is the total area enclosed by the geometry of the slider at macroscopic level, whereas real area of contact which is to be identified as exceedingly small fraction of apparent contact area at microscopic level. By perceiving this conception, various frictional models such as *Hertzian's model* and *Mindlin model* [10] were adopted on an assumption of surfaces being smooth i.e. when the real contact area during sliding is similar to that of apparent contact area

in the presence of insignificant adhesive forces. This work encouraged many researchers to understand the phenomenon of friction and wear from macro-scale to micro-scale and even moving towards nanotribology and since then there has been significant evolution in understanding the micro and even nano-level frictional properties of materials [11] and changed their outlook to consider the surface irregularities during sliding of surfaces. The geometry of these ridges and furrows profoundly influence the static properties namely electrical conductivity, optical phenomenon and thermal conductivity or dynamic properties as friction, wear and galling [8, 12].

In 1971, Johnson, Kendall and Roberts (JKR) [13] and Derjaguin, Muller and Toporov (DMT) [14] examined the effect of surface roughness incorporation of the action of adhesive forces over the sliding surfaces, as a result of this there was an inter-transmission of material over the surfaces furthermore this tendency of diffusion of material could be momentarily or perpetually and termed as adhesive wear. Bhushan [9] scrutinized the behavior of sliding surfaces and mathematically quantified the adhesive wear of sliding surfaces by introducing a term plasticity index ' ψ '.

The average pressure is given by,

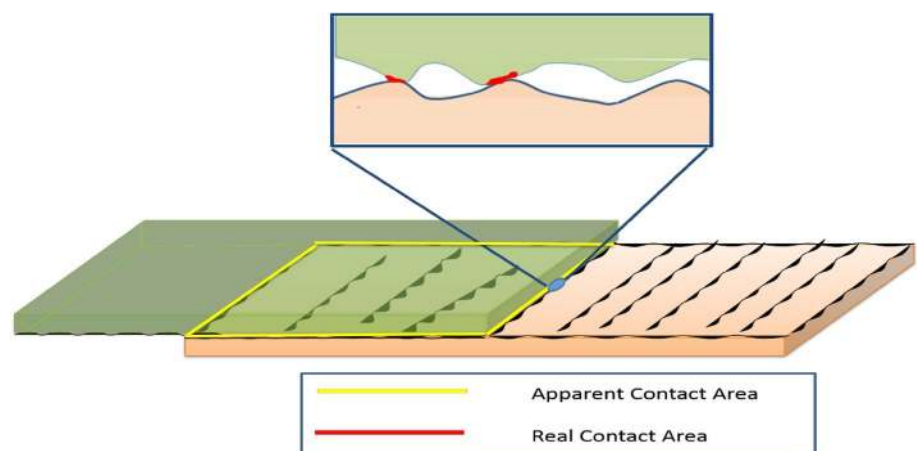
$$\sigma = \frac{F}{A} \approx \frac{1}{2} E^* \nabla z \quad (2)$$

During sliding, the transferred material might also be work-hardened and thus causing abrasive wear on the counter body when the applied load (Eq. 2) is greater than of hardness of the material (σ_0) along with greater magnitude of ' ψ ' i.e. if

$$\psi = \frac{E^* \nabla z}{\sigma_0} > 2 \quad (3)$$

Then, the micro-roughness of the sliding surfaces are in an entirely plastic state of deformation and results in the

Fig. 1 Understanding the basic fundamentals of mating surfaces



onset of sticking of materials to one another and hereby such a tribological behavior of surfaces is known as galling.

ASTM Standard G98-89 [15, 16], a prevailing experimental procedure to evaluate galling describes the phenomenon as a severe case of tribological behavior between two surfaces that are in contact where there is non-uniform material transfer that is not restricted within the system on a macroscopic scale. This, along with a thin film lubrication, intensifies the formation of surface protrusions under the action of loads at the interface of the surfaces with relative sliding and hence augments the galling tendency [16].

There are number of ways to deal with the concern of galling which includes modification of design with use of FEA models, varying microstructure of sample either by altering alloy composition or performing heat treatment and the use of various solid lubricant coatings either in terms of hard ceramic or use of low frictional coefficient polymer coatings. The use of superfluous fluorine coatings is most suitable method for curbing the galling tendency from the above mentioned mitigation methods.

The current state of the art interpreted from the search results obtained from the "Scopus" and "Web of Science" exemplifies that the topic of galling has been extensively covered by many researchers and are their significant work are have been published in the form of research articles, however, from the literature survey it is visible that although researchers have extensively inspected the phenomenon of galling and wear in association with the application of fluoropolymers, but the field lacks compilation of all the available literature which we have attempted to cover in the presented review. The present review elucidates the phenomenological aspects of galling, its effects on numerous engineering application from space to the biological implants along with the significance of various fluorine based coatings of PTFE, FEP, PFA, PVDF, ECTFE, ETFE and PEEK for anti-galling and wear resistant applications. Simultaneously, the present review also deals with the physical and mechanical properties of these fluoropolymers along with their synergistic effect with carbon nanofibers(CNTs), ceramics- $\text{Al}_2\text{O}_3/\text{TiO}_2$, modified nano- CeO_2 (MN- CeO_2), Polyamides (PA), polymethylmethacrylate (PMMA) and multi-walled nanocarbon tubes(MWNTs) for averting wear. The implementation of these mitigation techniques will help to achieve ease of functionality and the supreme degree of engineering precision and accuracy as required in diverse fields spanning from industry to defence.

2 Fundamentals of galling

Referring upon the definition of galling as adverted by ASTM G:98-89 [16], it is the plastic deformation of local contact points owing to high magnitude of contact load

and friction, as a consequence there is an inter-diffusion of material in-between the sliding surfaces as observed on a macro scale. In advance sections, the micro and nano-scale mechanisms of galling has been discussed in supplementary with nano-scale dynamics of galling concurrently, it also converses the number of factors that augments the dynamics of galling.

2.1 Galling mechanisms

From several decades many researchers had tried to scrutinize the fundamental aspects of the galling in which Komanduri and Shaw [17] were first to examine and conferred the various micro-mechanisms of galling in carbides systems during sliding of surfaces, namely:

I. Dislodgement, II. Disintegration, III. Disassociation, IV. Dissolution, V. Degeneration.

From the above mentioned galling mechanisms, the preceding two can be pronounced as mechanical in nature while the subsequent three can be characterized as both metallurgical and chemical. On the course of high-speed sliding, they observed that there was dislodgement of carbides phase from the matrix owing to the variation in their strain rate, incompatibility and incoherency in between them as there was plastic deformation of the matrix, whereas the hard and brittle second phase carbides deforms elastically. As an outcome, there was a depletion of distinct phases that eventually lead to the disintegration and micro-fracture of carbides on the surface, hence increasing the tendency towards galling.

During the course of high-speed sliding, there was augmentation in the interfacial temperature in between the sliding surfaces, which marks the dissociation of surface carbides and concurrently these dissociated carbides gets oxidized to give end product as metal oxide (MO_2), amorphous carbon or carbon dioxide (CO_2) [18]. In addition to carbide, there are inclusion of various cubic carbides stabilizers such as Chromium, Tungsten, or Molybdenum. At augmented interfacial temperature there is disintegration and dissolvent of unstable orthorhombic and hexagonal carbides into matrix owing to the oxidation of elements as stated above results in wear of the system [17].

Schedin [19] scrutinized the fundamentals and mechanism of galling for Zinc-Coated tool steel with sheets during the forming process and stated that during sliding, the tool surface contour infiltrate the sheet surface and leads to the formation of plastic waves, as a consequence there is direct transfer of thin layer of sheet material on the surface of tool with or without generation of unrestrained debris, that can be accrued at different spots on the tool surface which results in galling, hence the geometry of the mating surfaces plays a significant role in initiating galling, plowing or cutting as depicted in Fig. 2a that illustrating

source of the plastic wave in regular frictional mechanism. Figure 2 also, depicts the schematics of galling mechanisms that was witnessed during the forming process. Figure 2b illustrates the initial stage of galling observed during the movement of tool surface over sheet asperities and peculiarly noticed in areas having surface abnormalities such as grinding smears assimilated during surface preparation, scratches owing to the indecorous handling of engineering products, surface abrasions throughout the testing of final products, or during the plowing or cutting of hard particles either from sheet material or foreign particles [19].

Over the early flow of plastic waves over the interaction of the tool and sheet surface that asserts tool surface contours to intrude into the sheet surface at places where there is breakdown of lubrication film that eventually leads to plastic working, yielding and adhesion of subsurfaces as presented in Fig. 2c. Over the continual passes under the impact of high pressure, there is transfer of material and enlarging of mass into large fragments sufficient to seize up the system as shown in Fig. 2d.

Researchers had also tried to find out the correlation between the frictional heating and the phenomenon of galling at contact asperities prior to that researchers had already scrutinized the frictional behavior of sliding surfaces by performing numerous experiments. During the experiments, they rotated vertical bar against the flat plate at low sliding velocity that resulted in the generation of heat which is a function of temperature and represented in the following Eq. (4) in which 'R_s' is the radius (m) of

contact, v is velocity (m/s) and HV is the hardness value (Pascal) of sheet [20, 21]

$$q = \frac{\pi}{2} \mu v R_s^2 HV_{sheet} \tag{4}$$

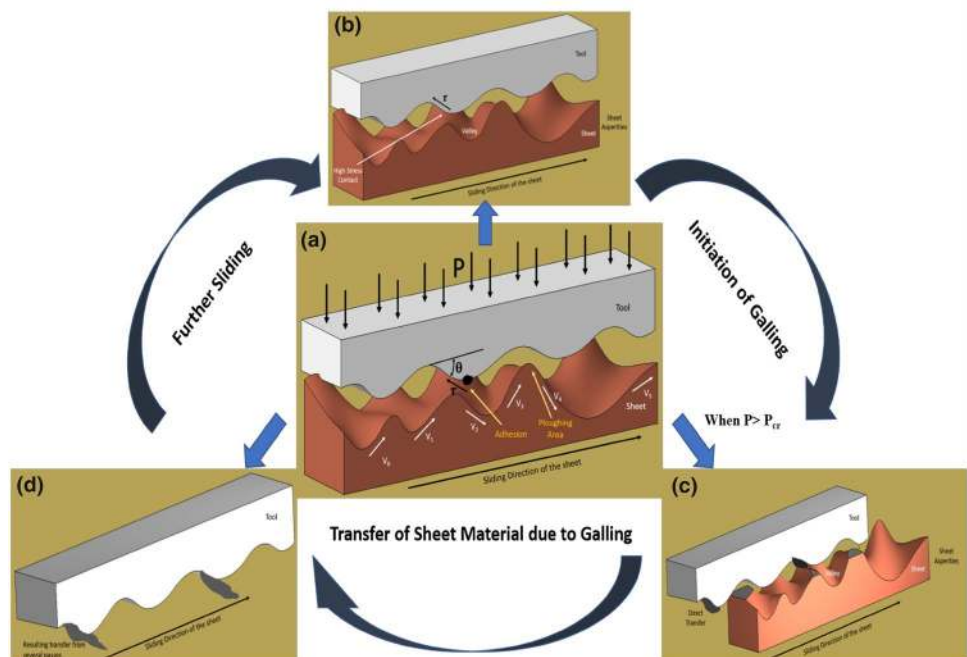
$$T_f = \frac{q}{(\sqrt{ab} K_{eff})} \tag{5}$$

From Eqs. (4) and (5) we get,

$$T_f = \frac{\frac{\pi}{2} \mu v R_s^2 HV_{sheet}}{(\sqrt{ab} K_{eff})} \tag{6}$$

The Eq. (5) deals with the above stated heat generation (q) due to friction during sliding of surfaces, the flash temperature 'T_f' of in between lubricating film and the effective thermal conductivity 'K_{eff}' (W/m/K) of the sliding of surfaces. They made some assumption that contact is semi-ellipsoidal in which a and b signifies the length of semi-axes in and normal to the direction of sliding also it's the function of the thermal properties of the conducting contact surfaces. Further, for a lubricated tool-sheet contact, the provision for commencement of galling can be articulated as if T_f > T_{cr}, where 'T_{cr}' is the critical temperature of the lubrication owing to the high heat generation during sliding. As a consequence there was a failure of thin lubricating film and initiation of transfer of material to boundary lubricated sliding contact from the region of

Fig. 2 Macro-galling mechanism. **a** Development of a plastic wave during the interaction between stiff-tool and deformable sheet. **b** Removal and sticking of material in the course of the initial mating of surfaces. **c** After the early contact. **d** After several passes



relatively low coefficient of friction value to the region of the relatively high value of friction coefficient [22].

Equation (6) depicts that the amount of heat generated during sliding depends on the material surface properties such as the sheet hardness. Flash temperature is proportionate to the hardness of the surface and is inversely proportionate to the thermal conductivity of the material.

$$K_{eff} = 2.746K_t + K_s \left[10.379 + 7.603 \left(\frac{av}{\alpha_s} \right)^{1.158} \right]^{0.432} \quad (7)$$

The prevailing equation needed during calculation of effective thermal conductivity is defined by Eq. (7), in which the subscripts “t” and “s” relate to the tool and the sheet respectively, and α_s is the thermal diffusivity of sheet material. Upon unpretentious increase in tool conductivity, there is a significant drop in the flashpoint, which circuitously descends the probability of galling. Therefore, thermal conductivity of the system plays crucial role in the selection of surface coating material for forestalling the phenomenon of galling, e.g. with the application of surface coating possessing high value of thermal conductivity increases the possibility to drop the furthestmost flash temperature to adequate numeral, less than the critical temperature owing to increase in anti-sticking possessions, thus galling can be avoided in various engineering applications [22].

Karlsson et al. [23] had described that the transference of material not only observe at localized precincts with the highest contact pressure, but it also takes place at

the areas owning high magnitude of plastic strains. The authors stated that the whole phenomenon of wear and galling during sliding can be discussed under the umbrella of friction and critical pressure and had reported it in three stages, the first phase was illustrated as a stable friction stage, and subsequently further sliding caused frictional value to upsurge in stage II. Further sliding led to the beginning of stage III, accompanied by high and instable frictional value as illustrated in Fig. 3.

During commencement of sliding, there is a diffusion of reedy layer of material from the subsurface of sheet towards the tool-surface. This preliminary adhered thin film of sheet material was unstable and incapable to sustain its prolonged adherence, thus as an outcome it's back transferred from tool surface to sheet subsurface resulting in trivial deviations in frictional value as observed in stage I. Further progression in sliding induces the onset of stage II that leads to rise in diffusion rate among sheet and tool subsurfaces owing to the rise in the value of friction coefficient which results in the formation of microscopic lumps that caused scratches and microscopic plowing over sheet surface. The transition from adhesion mechanism to the commencement of wear in stage II has been comprehended as the foreboding of galling [23].

During stage III, there was stern adhesive wear of sheet surface, followed by complete diffusion and adhesion of sheet material that resulted in the formation of macroscopic wedges on the tool surface, consequently the high and unstable value of friction was observed, this occurrence is known as galling. Throughout the stage, there was no significant change in the microstructure

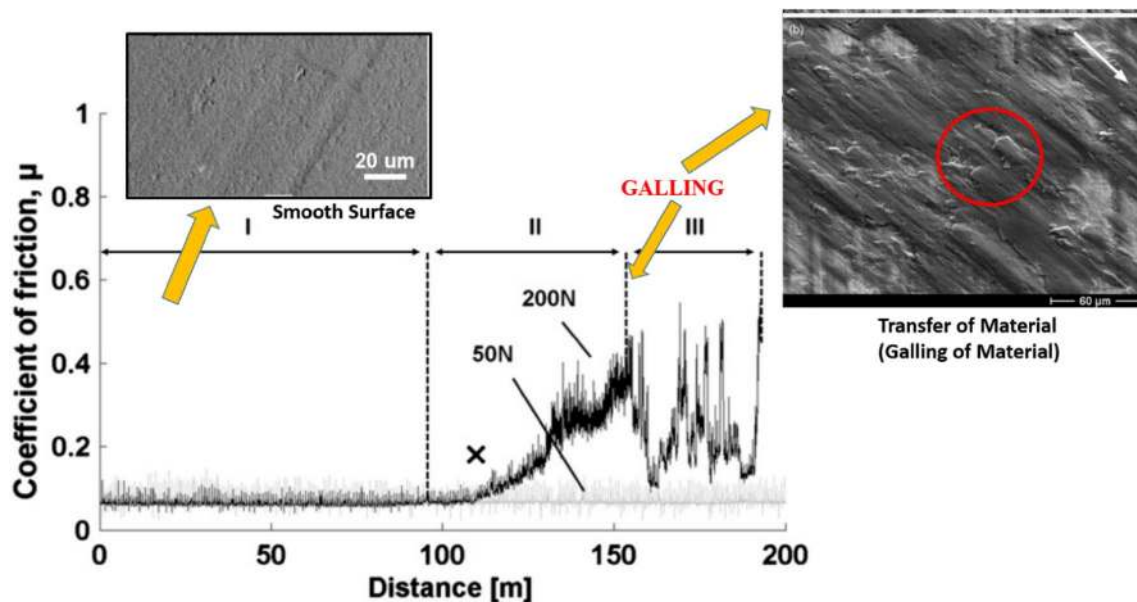


Fig. 3 Illustrating different stages during friction test (Refs. [24–26] copyright from Elsevier)

of the tool, therefore it had scarcely influence on the galling action. Hence, the author's concluded that wear mechanisms observed during stage I and stage II and the transition between the stages are of high interest for the understanding of the influence of tool steel microstructure on galling origination [23]. This significant research ignited the curiosity of many researchers to further scrutinize the fundamentals of galling not only under the action of friction but also to be consider effectuate of applied load. Dong [27] and his team experimented and tried to probe the corollary of applied contact pressure along with the sliding distance on macro-galling. They stimulated sheet metal forming process and performed the tests through square cup drawing method and their elucidations has been summarized in the Table 1.

Dong [27] and his team also tried to understand galling at atomic level, and established atomistic galling mechanism at drawing die(coated with TiC)-workpiece(α -Fe) interface by adopting first principle calculations. For establishing interface model, TiC (100)/ α -Fe (110) interface was chosen as a most stable surface between TiC and Fe, owing to the optimal values of lattice constant, bulk modulus, surface energy (as compiled in the Table 2) and the lattices depicting lower mismatched.

They calculated the work of separation for interface and sub-interfaces for TiC (100)/ α -Fe (110). The work of separation is defined as the optimal value of work given at interface to separate it into two free surfaces at the interface, which is given as:

$$W_{sep} = \frac{A(E_{interface} - E_{Fe-fixed} - E_{TiC-fixed})}{2} \quad (8)$$

where "A" is the area of contact at the interface, $E_{interface}$ is the total energy possessed by the system during sliding, $E_{Fe-fixed}$ is the total energy possessed by the disengaged slab for Fe and $E_{TiC-fixed}$ is the total energy possessed by the disengaged slab for TiC. From Eq. (8) they obtained the values of work energy for TiC/Fe interface as 4.51 J/

Table 2 Theoretical and practical value of lattice constant, bulk modulus and surface energy for TiC and Fe

Material	Lattice constant (Å)	Bulk modulus (GPa)	$\gamma_{(110)}$ (J/m ²)	$\gamma_{(100)}$ (J/m ²)	
TiC	4.38	252	1.68	3.66	Theoretical
	4.33	241	–	–	Experimental
Fe	2.84	173	2.49	2.22	Theoretical
	2.86	172	–	–	Experimental

m² which was 2.29 J/m² (as shown in Fig. 4) greater than that of surface energy of α -Fe, imputing that it is easier to break bonds of Fe subinterface upon work separation than to disintegrate bonds at the interface and as consequence, there was potential separation at Fe subinterface along with diffusion of Fe atoms towards TiC slab owing to strong adhesive energy at TiC(100)/ α -Fe on application of external loads. They reported that it could be a possible atomistic reason for the adherence of steel sheet towards die in sheet metal forming process [27].

From the various galling mechanisms discussed above, it can be concluded that the overall result from all the transitions is rubbing between two materials, leading to transfer and localized adhesion between them, and ultimately causing the phenomenon of galling. The rate of galling can be enhanced or diminished with the change in several factors as covered in the next section.

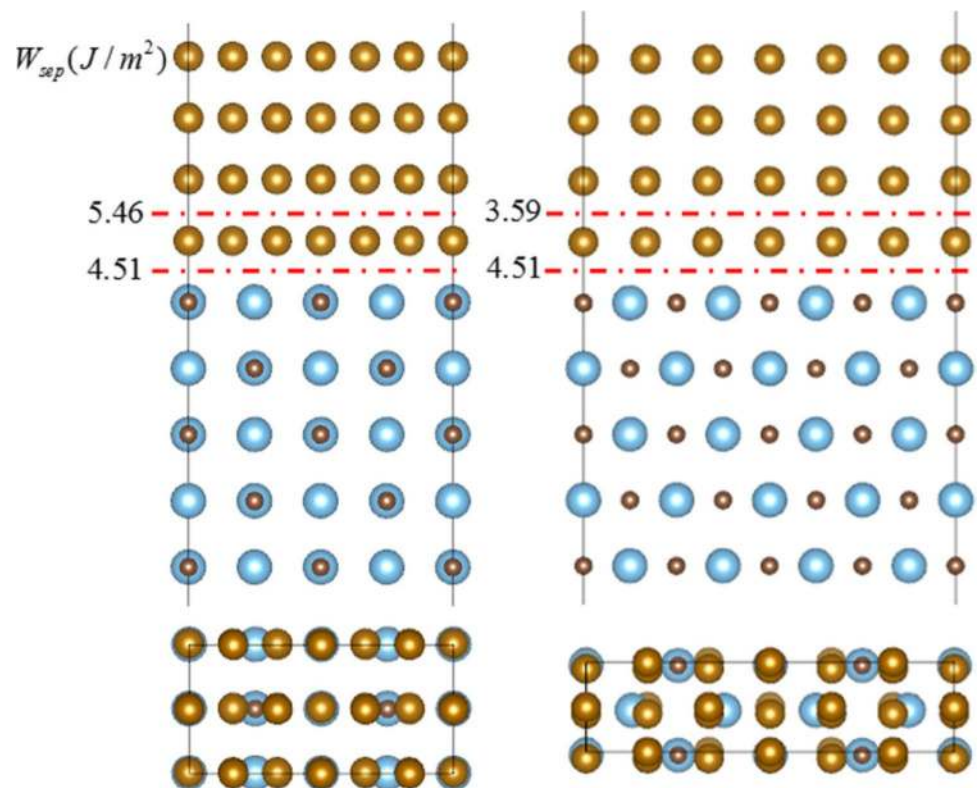
2.2 Factors governing the phenomenon of galling

The mechanisms discussed above for the phenomenon of galling are subjected to various tribological, mechanical and metallurgical factors, such as designing abnormalities of product/specimen, the material used for the product along with its morphological properties, in particular, their microstructure and surface texture. Also, alteration

Table 1 Abridgement of the experiment performed Dong et al. and their observations

Sr. No.	Various considerations on galling behavior	Observations
1	Effect of drawing cycle on the galling when increased from N=1 to N=15	Upward growth in the galling behavior on the die surface, while there was downward galling on drawn cup surface owing to ploughing effect
2	Effect of critical contact pressure and effective sliding distance	When the applied contact pressure and sliding distance is greater than or equal to the critical contact pressure (P_{cr} =240 N) and Effective sliding distance (S_E), evokes the instigation of Galling
3	Effect of die height	Galling behavior augmented when die height increased from 10 to 20
4	Region on die which was severely prone to galling	0° to 70° on die radius showed severe galling

Fig. 4 Diffusion of atoms during galling over influence work separation (Ref. [27] copyrights from Springer)



in environment and corrosion highly influences the rate of galling during the mating of two dynamic surfaces.

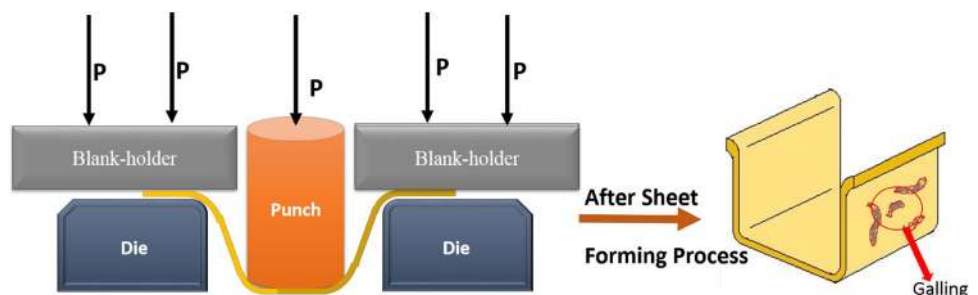
2.2.1 Pothole in design of sheet metal forming contributing galling

Sheet metal forming is the manufacturing process where finished product is obtained deprived of machining, instead the configuration of sheet is varied and bend to the anticipated form under the action of external applied load and these imputed stresses are having the magnitude above the yield strength value of material and below the failure strength, hence inducing material to deform plastically [28] as depicted in Fig. 5.

The influence of inappropriate load distribution resulting in galling. The balanced load distribution results in

stable equilibrium, with the use of different tools such as basic science, mathematics and engineering sciences that inhibits failure of the product. Bruschelli et al. [29] practiced finite element method (FEM) to understand the load distribution over the fasteners and reported that during fastening, there is non-uniform distribution of load during make-up and break-out process and concluded that the failure position is restricted at the ends of the tubing owing to high stress concentration. After analysing the FEM, researchers and established the relationship between plastic deformation of material and the stress applied towards galling. Guangjie et al. [30] performed finite element analysis for understanding the phenomenon of galling in which the material was a piecewise linear-plastic model using the theory of plasticity i.e. Von-Mises or maximum distortion energy criterion of yielding

Fig. 5 Imperfection in design of die leads to galling



condition. After understanding the bottlenecks in design of the threads (fasteners) through FEM, researchers modified the design of the threads in such a manner they were able to withstand the applied load without getting plastically deformed and hence averting galling.

During whole manufacturing process, the tool design has a significant role in the initiation of galling and it is highly vulnerable to the surface roughness of tool (without coating) rather than surface irregularities of the sheet [31]. Zhou et al. [32], Yangui et al. [33] and Dong et al. [27] in this context researchers had reported that the commencement and progression of galling originates at the mould radius (i.e. around 0° to 70°) during forming process during which there is a severe plastic deformation of sheet metal, inducing adhesion of sheet material to the surface of the tool and hence galling occurs. The die with sharp, fine and rigid curving ridges correspondingly enhances the effect of galling [34].

2.2.2 Material properties

For most of the engineering applications the selection of material is adopted subsequent to the design finalization owing to its various intrinsic and extrinsic properties vacillating from macro-level to nano-level and even to atomic level. Also the scientific community of twenty-first-century has been inspired by the nature to have meticulous knowledge of material and their properties, viz., optical such as color, luminosity, and refractive index, surface factors such as surface tension, surface energy and corrosion, electric such as dielectric constant, or mechanical such as strength, toughness, surface roughness and ductility and hence started to bio-mimic, namely composite, body armor, Nacre (the iridescent material), 3D Emulated fiber, thermally stable and hydrophobic coatings [35–43].

The above discussed properties ominously affects the galling tendency of material, for e.g. materials that have high ductility and less hardenability will try to deform plastically, and thus burgeoning the contact area of rough surfaces leading to inception of galling, whereas the material possessing low ductility and high hardness will have high galling resistance properties. Subsequently, under the application of immense pressure, the surface asperities have a tendency towards fracture, resulting in the commencement of flakes, alternatively getting adhered to the counter body. Thus, diminishing the probability of galling, but instantaneously these small flakes augment surface wear owing to high rate of abrasion and erosion of surfaces.


2.2.2.1 Microstructure Microstructure can be defined as the arrangement of a prepared surface of material as exposed by a microscope superior to $25\times$ magnification

revealing the grain size, and these microstructure substantially influences many characteristic properties of the material such as thermal and electrical conductivity, specific heat of capacity, corrosion resistance, strength, and hardness. During sliding, the surfaces possessing coarse grain structure (greater than $1.2\ \mu\text{m}$) leads to the amplification of the adhesion tendency hence augmenting the galling [44, 45]. This tendency of material adhesion is also influenced by the divergent prearrangement of atoms, since crystal arrangement of face-centered cubic (FCC) has a high proclivity towards plastic deformation at inferior applied loads and hence the high rate of material diffusion is observed than a body-centered cubic (BCC) crystal arrangements. The reason is that BCC crystal structure having limited number of closed-pack planes and their configuration is such that they mutually impede the dislocation movement make them difficult to move, thus BCC is more brittle as compared to FCC crystal structure [46, 47]. It is also observed that during sliding, with the application of high magnitude of load, the skin-deep FCC material transforms into hexagonal close-packed (HCP) crystal structure having one of its planes $\{0001\}$ oriented themselves to the worn surface [48].

The redundant behavior of material during plastic deformation has been perceived i.e. the movement of dislocations from one plane to another plane, known as cross slip and the rate of cross slip is the function of the stacking fault energy (SFE). SFE is the energy acquired by the crystal structure owing to the discontinuity in the stacking planes or closed-pack plane carrying the partial dislocations in crystal structure. These partial dislocations can either be Schottky type, having the direction of Burger vector parallel to the plane of stacking fault, or of the Frank type, having the direction of Burger vector normal to the plane of stacking fault [46]. The cross slip dislocations movement is inhibited by the presence of defect, which arises because of high stacking fault energy. This high amount of stacking fault energy exhibits a smaller number of restraining stacking-faults and low strain hardening rate hence augments the tendency of dislocations to move from one plane to another (cross slip) under an applied load, owing to the phenomenon of galling. The SFE of some common elements and tendency has been illustrated in Table 3.

The commencement of galling is also a function of the c/a ratio for HCP crystal structure. In Hexagonal Close-Packed (HCP) structure atoms are arranged in a sequence 'ABABAB---'. Therefore 'c' which represents the distance between two identical layers 'a' is no longer independent. Primarily, HCP structure has a fixed c/a ratio [53, 54]. The HCP structure acquiring large value of c/a ratio has a truncated rate of cross slip during dislocation movement over the basal plane than along the pyramidal and prismatic planes during the application of pressure, hence

Table 3 Stacking fault energy of some common materials and its effect on galling [36, 49–52]

Metal/alloy	Stacking fault energy (mJ m ⁻²)	Effect on Galling
Gold (Ag)	20–30	 Galling Tendency Decreases
SS 316	42	
Silica (Si)	50	
Copper (Cu)	70–78	
Nickel (Ni)	90	
Magnesium (Mg)	125	
Aluminum (Al)	160–200	
Zirconia (Zr)	240	


less vulnerable towards galling and therefore owing to this understanding there has been severe galling reported in titanium alloy sheet forming process, as titanium alloys acquire low magnitude of c/a , that leads to the effortless movement of dislocation by virtue of cross slip [55] and leading to the abatement in the strain hardening rate and hence severe plastic deformation has been observed [56, 57], while against cadmium-based alloys and cobalt-base alloys, as they are less vulnerable and having high degree of anti-galling property than titanium alloys. Also, there is a curtailment in the SFE with the substitution of Nickel in cobalt-base alloy system as a consequence, there is a retrenchment in the strain hardening rate and the stress at which the cross-slip occurs along with the rise in the plasticity and hence the impression of galling is severe. Abridgment from Tables 3 and 4 illustrates the influence of SFE and c/a ratio on galling tendency, as with the increase in the ratio will result in depressing the SFE value and hence constraining galling.

Therefore, the stacking fault energy and c/a ratio plays a crucial role during the selection of enhanced anti-galling coating where the coating material should be acquiring lower value of SFE and high c/a ratio [55].

2.2.2.2 Surface topography The topography or the texture of the materials sternly influences several physical properties and chemical properties such as friction and corrosion resistance. The material surface can be characterized as the function of lay, surface roughness and waviness that implements a vital role during juxtapositioning of surfaces both in static and in dynamic states. These surface textures results in the increased in magnitude of friction as discussed above and hence galling.

Podgornik et al. [26, 58] had conducted various experiment and comprehend relationship between the roughness of the sliding surfaces and the phenomenon of galling along with various other tribological properties of the

Table 4 The c/a ratios for some common metals at room temperature and its effect on galling

Metal	c/a Ratio	Effect on Galling
Cadmium (Al)	1.886	 Galling Tendency Decreases
Zinc (Zn)	1.856	
Ideal HCP	1.633	
Cobalt (Co)	1.632	
Magnesium (Mg)	1.623	
Zirconia (Zr)	1.593	
Titanium (Ti)	1.587	
Beryllium (Be)	1.568	

sliding surfaces. Initially, the surface was prepared of surface roughness varying from $R_a \approx 0.25$ to $0.02 \mu\text{m}$ with the aid of shot peening, grinding and polishing with different grades and tested under load-scanning rig apparatus (as shown in Fig. 6).

During the experiment, the twin cylindrical slider of diameter 10 mm and height of 100 mm were slithered against each other at a steady velocity of 0.01 m/s and concurrently the applied load was gradually increased from 100 to 1300 N. After the experiment they scrutinized the experiment results and observed that at surface roughness (R_a) ≈ 0.25 and the coefficient of friction as 0.3, it lead to the prohibitive magnitude of plasticity, increased rate of adhesion of sliding surfaces than the surfaces attaining surface roughness magnitude of $R_a \approx 0.02$. The reduction in the roughness value resulted in the lowering the friction coefficient from 0.3 to 0.1 and as an outcome, there was a decline in amount of adhesion of material and accordingly minimize the galling. Hence, the materials having lower magnitude of surface roughness and friction can be selected as a coating material for anti-galling applications [26].

2.2.2.3 Surface hardness Surface hardness can be defined as the resistance to the concentrated plastic deformation observed during mechanical indentation or abrasion [59]. Clark [60] did experiments and established affiliation inbetween the influence of surface hardness of the sliding surfaces and the tribological phenomenon of galling. For achieving surface hardness, the surface was diffused with carbon atoms through the process of carburization. Individually, the untreated and carburized surfaces were experimented under skindmore tension tester and a torque wrench apparatus for obtaining the value of yield strength and torque applied at 50%, 75%, and 90% yield value and hence the hardness via following equations:

$$T_y = \frac{kF_p d}{12} \quad (9)$$

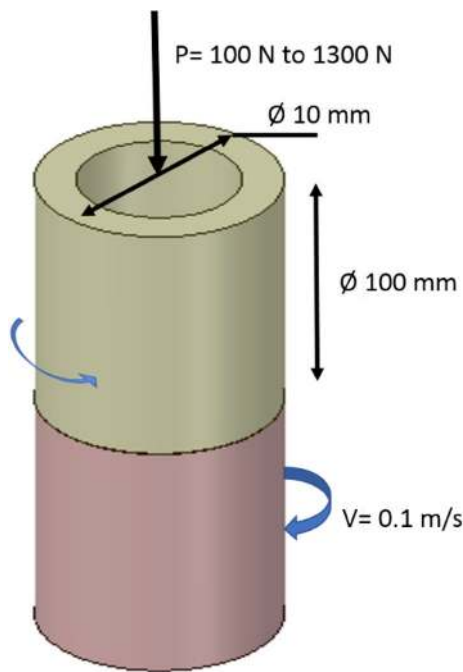


Fig. 6 Load-scanning rig apparatus to check the effect of surface topography on Galling

$$\sigma_y = \frac{T_y(12)}{kdA_b} \quad (10)$$

From above Eqs. (10) and (11),

$$T_y = \frac{\sigma_y kdA_b}{12} \quad (11)$$

where,

After scrutinizing the results obtained by the author it can be concluded that during the decrease in the magnitude of force from 4000 to 1000 lbs after the (1) seventh loading cycle at 50% yield, (2) 14th cycles at 75% of load and (3) 19th loading cycles at 90% of yield for untreated fasteners, had high magnitude of friction coefficient (μ) overhead the standard magnitude of 0.8, which was an indication of commencement of galling. Though, for carburized treated surfaces, there was also reduction in the load at various yields but the reducing values were not less than the standard threshold value ($\mu = 0.8$) that was required for the commencement of galling, illustrating that the specimen having low surface hardness value has greater propensity for adhesion and are more vulnerable to galling under high applied loads. Hence, galling results in a decrease in strength, toughness, of seizure components, change in tool geometry, cause tearing at the distinct strained area and ultimately failure of a material

and loss of material adds to the economy of the nation. Many researchers had studied the wear phenomenon in bio-implants such as knee replacement, hip replacement, shoulder replacement and fasteners used to assemble the orthopedic joints in the human body and concluded that effect of galling in bio-implants results in failure of a component that is a serious issue of concerned [58, 61, 62]. Therefore checking and monitoring the galling in numerous engineering components is a vital need, some of them are refining of tool design, surface treatment of the sliding interfaces or application of lubricous coating over the surfaces. With reference to the scope of this review article authors have discussed the wear resistant properties of flouropolymers.

3 Selection of the coating material

From the above discussed various fundamental parameters such imperfect designs, surface microstructure and surface-roughness, hardness and friction coefficients governs the galling resistance of the sliding surfaces and it is difficult to prepare sliding surfaces possessing lower value of SFE, surface roughness and friction coefficient and high hardness concurrently, therefore researchers had tried to modify surfaces by the application of top coat on the sliding surface that encloses all of the desired characteristics as discussed above. Researchers tried numerous material as surface coat for enhancing anti-galling properties such as hard inorganic coatings of TiC, DLC, VN, graphite, hBN or organic coating of paraffins, microcrystalline, carnauba, polyethylene and amide waxes. Out of the above-mentioned, polytetrafluoroethylene (PTFE) and polyamides have good lubricating property owing to their plastic or viscoplastic behavior under applied frictional loads [63–70].

Global Fluoropolymers Market was valued at \$5404 million in 2015, and is expected to reach \$9034 million by 2022, registering a CAGR of 7.7% from 2016 to 2022 [71]. The foremost patent on fluoro-based polymers was claimed by IG Farben in 1934 of polychlorotrifluoroethylene (PCTFE) but owing to its limited applications, in 1938 Plunket [72] discovered Polytetrafluoroethylene (PTFE) that increased the interest of researchers to further scrutinize the various properties of fluorine-containing polymers and has copious applications namely conductive polymers, biomaterials, optical fiber, surfactants and fire-fighting agents, elastomers, paints and coating materials [73–76] as depicted in Fig. 7.

Hence fluorine-based polymers are recognized as great value-added molecules owing to their versatile unique feature particularly low value of refractive index, cohesive energy, surface energy and relative permittivity, and high

value of thermal resistance, high chemical stability, resistance against UV, concentrated mineral acids, alkalis, and aging [76–78]. The tradename of commercially available Fluoropolymers has been tabulated in Table 5. But owing to the scope of this review article, authors had primarily focused on the application of these fluoro-based polymers for wear resistance, lower frictional and anti-galling coatings.

3.1 Polytetrafluoroethylene (PTFE)

PTFE (commercially known as 'Teflon[®]', Dyneon[™], Hyflon[®], Fluon[®], Hostaflon, Chemfluor, Algoflon[®]) is a

thermoplastic that owns high thermal stability, chemical inertness, non-adhesive, uniform distribution in resin, corrosion resistant [83] and lowest value of friction coefficient and high load carrying capacity. DuPont, 3M, Solvay, AGC are the prime manufacturer of PTFE in the world [84, 85]. PTFE is a linear polymer of tetrafluoroethylene (TFE) (Fig. 8). In carbon–fluorine polymers, two fluorine atoms are covalently bonded to the single carbon atom reducing the C–F bond length from 1.42 to 1.35 Å that augments the stability of the polymer with average molecular weight of 400,000 to 900,000 g/mol. Its streamlined columnar configuration with a weak interactivity inbetween the molecules is one reason for easy slip during deformation

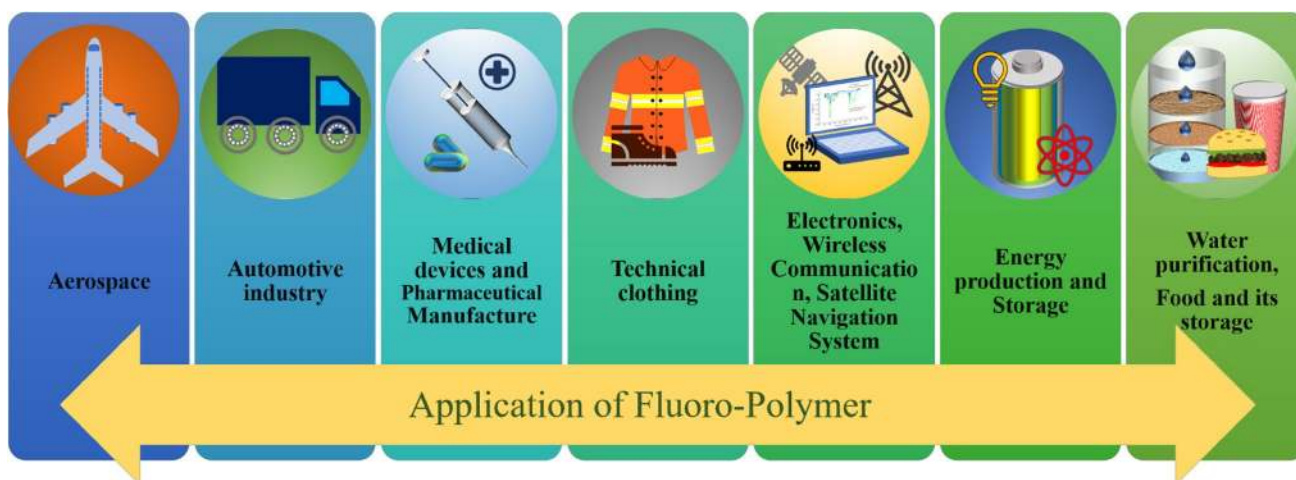


Fig. 7 Numerous application of fluoro-based polymers

Table 5 Tradename of commercially available fluoropolymers [79–82]

Fluoropolymer	Trade names
PTFE (polytetrafluoroethylene)	Sold by AGC under the tradename Fluon PTFE; Sold by Dupont and Chemours Company under the tradename Teflon; sold by Solvay Specialty Polymers under the tradenames Algoflon Hyflon and Polymist; sold by Daikin under the tradename Polyflon
PVF (polyvinylfluoride)	Tedlar
PVDF (polyvinylidene fluoride)	Kynar Solef Hylar
PCTFE (polychlorotrifluoroethylene)	Kel-F (3M), Neoflon (Daikin)
PFA (perfluoroalkoxy polymer)	Sold by AGC under the tradename Fluon PFA. Sold by DuPont under the tradename Teflon. Sold by Solvay Specialty Polymers under the tradename Hyflon. Neoflon (Daikin)
FEP (fluorinated ethylene-propylene)	Sold by DuPont under the tradename Teflon FEP. Also known as Neoflon (Daikin) and Hyflon
ETFE (polyethylenetetrafluoroethylene)	Sold by AGC under the trade name of FluonETFE Tefzel, sold by Daikin under the tradename Neoflon
ECTFE (polyethylenechlorotrifluoroethylene)	Halar sold by Solvay Specialty Polymers
FFPM/FFKM (Perfluorinated Elastomer [Perfluoroelastomer])	Kalrez. TecnoflonPFR DAI-EL (Daikin)
FPM/FKM (Fluorocarbon [Chlorotrifluoroethylenevinylidene fluoride])	Viton, Tecnoflon FKM, DAI-EL (Daikin)
PFPE (Perfluoropolyether)	Sold by DuPont under the tradename Krytox. Sold by Solvay Specialty Polymers S.p.A. as Fomblin and Galden

(as shown in Fig. 8) as PTFE has lowest friction coefficient ($\mu \sim 0.02$ to 0.04) among all the polymers [86, 87], eventually this makes PTFE a suitable candidate for the vacuum, non-flammable, hydrophobic and high temperature applications. At High temperature and pressure, these PTFE particles react to base metal in order to produce a thin lubricating film of metal-fluoride, hence augmenting the abrasive-wear resistance [88, 89] and thus making it an ideal aspirant for anti-galling applications [90].

Numerous researchers had tried to explode/explore this vital characteristics of fluorine based polymer and integrate them with the existing coatings. Initially a patented method was promulgated by Meng et al. [91] and Wang et al. [92] whereupon they formulated nano-copper ethanol colloidal, similarly a definite proportion of colloidal was prepared by mixing powdered PTFE nanoparticle (nano-PTFE) with epoxy and fetched a coating material of nano-particulate anti-friction (NPAF).

Meng et al. [93] had performed numerous experiments and tried to validate the anti-friction, anti-wear and anti-galling characteristics of NPAF coating, during which the NPAF coating material was prepared about 6 g of PTFE particles of diameter 591 nm and 15 g of Polyacrylic acid resin and then applied on manufactured buttress thread couplers and then tested for make-up torque as make-up torque is the function of the probability of galling in which higher the magnitude of make-up torque, the higher is the contingency of thread galling [30, 91, 94–99]. After scrutinizing the data obtained by the after-experiment, they reported that there was a significant drop in the magnitude of make-up torque from 19,426 to 145,638 Nm i.e. 24.65% in NPAF coated threads than to uncoated treaded and hence, they elucidated that these incorporated nano-PTFE particles were able to control the pre-plastic deformation of threads owing to the decrease in make-up

torque prior to the critical value of torque, exhibiting anti-galling characteristics [90].

Srinivasan et al. [100] reported that the application of electroless composite coating of the nickel–phosphorous and PTFE (Ni/P-PTFE) on the sliding surfaces had augmented the anti-galling characteristics of the surface. Electroless method is most widely used for applying these synergistic coatings on substrate owing to its high durability, cost effective and excellent anti-galling characteristics [42, 101–104]. This research encouraged researchers to have synergistic coatings incorporating PTFE particles of size $0.3 \mu\text{m}$ along with other elements, that resulted in the reduction of magnitude of the frictional coefficient from 0.07 to 0.035. During an experiment, they did electroless coating of the Ni/P-PTFE on low carbon steel plate of $50 \text{ mm} \times 25 \text{ mm} \times 2 \text{ mm}$ and ball-on-disc tribometer was exerted for the measurement of tribological properties of the applied Ni/P-PTFE coating and the thickness of functional coating was $5 \mu\text{m}$ as measured by X-ray fluorescence. They varied the concentration of PTFE from 0 to 27.6 vol% and tried to calculate the volumetric wear (R_w) during the tribometric experiment for varying concentration of PTFE. The volumetric wear was calculated by

$$R_w = V/F * S \quad (12)$$

where “F” is the applied force (N), “S” is the sliding distance (m) and “V” is wear volume (mm^3) which was achieved through the non-contact surface mapping profiler.

Following the experiment, the results were scrutinized, and they observed that there was palpable continuous drop in the magnitude of the friction coefficient from 0.31 to 0.12 with the increase in the PTFE concentration after the sliding distance of 50 m. Similarly there was also a drop of 15% (approx.) in the magnitude of the wear rate from 6.48 to 5.33 mm^3/Nm with an increasing volume of the

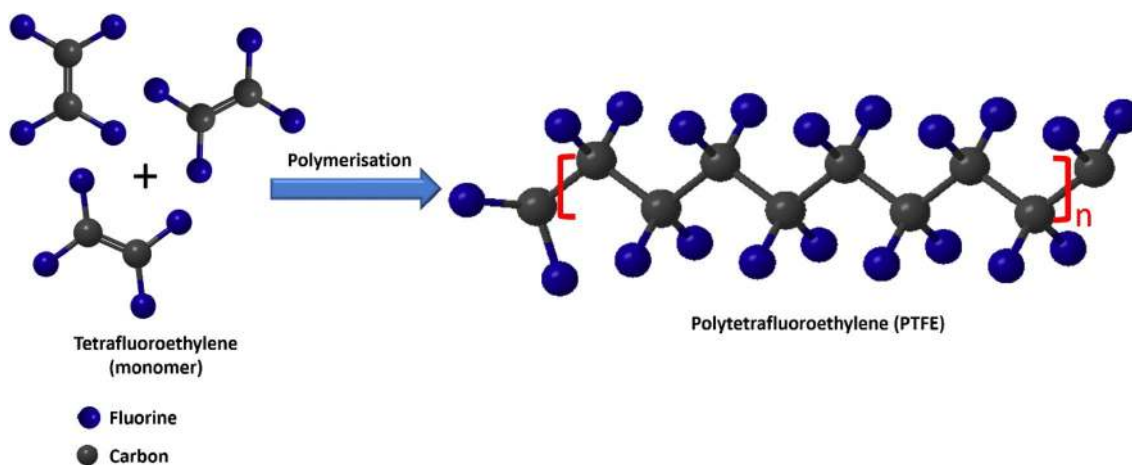


Fig. 8 Molecular streamline columnar structure of polytetrafluoroethylene (PTFE)

incorporated PTFE particles amidst the composite coating, this can be ascribed to PTFE particles that assimilated in the matrix that was diffused to the sliding surface by the shear force and created a thin lubricating film and resulted in augmenting the lubrication around the sliding surface and hence decreasing frictional coefficient and wear volume of the composite coating during the process with compromising the hardness as it also decreased from 506 to 323 Hv around 36%. The increased in the volume concentration of PTFE also improved the corrosion resistance characteristics of the system, results obtained by the polarization curve stated that there was a decrease in the magnitude of anodic Tafel slope β_a from 0.162 to 0.098 V/decade, cathodic Tafel slope β_c from -0.148 to -0.114 V/decade and there was decreased in corrosion current density (I_{corr}) from 3.75×10^{-3} to 1.21×10^{-6} A/dm². The abridgement of the experimental results has been represented in the Table 6 and Fig. 9, depicting the effect of augmenting the volume concentration of PTFE in the coating matrix on various surface characteristics such as friction coefficient, hardness, wear rate corrosion resistance that governs the galling mechanism [83].

Although by increasing the volume concentration of PTFE augments the various characteristics of the surface that improves the anti-galling properties, but it has limitation of addition which was reported by Zhao et al. [105]. They scrutinized the effect of varying contain of PTFE in Ni/P composite coating and reported that at optimum concentration of PTFE in the matrix contributes in uniform distribution of hardness over the sliding surface owing to its uniform dispersion of PTFE and hence it conduces optimal anti-galling properties. On addition of further PTFE over the optimal level, there was inhomogeneity in the value of hardness over the surface owing to the agglomeration and settling out of the particles resulting in the decrease in anti-galling characteristics.

Researchers had also tried to establish the various amalgamations of PTFE with different inorganic particles such as silver, copper or MoS₂ to improve the anti-galling characteristics of the surface. Sieh et al. [106, 107] reported that the use application of electroplated non-cyanide Ag-PTFE coating has augmented the tribological performance of coating by providing constant

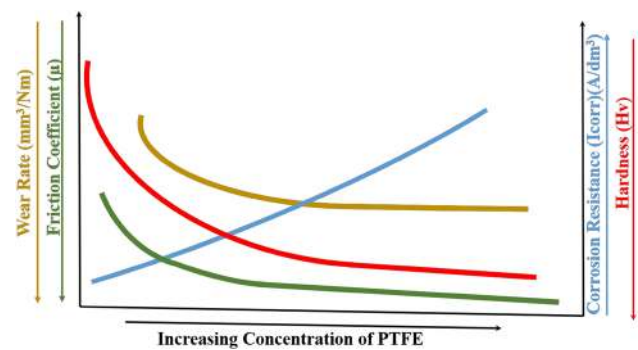


Fig. 9 Effect of augmenting concentration of PTFE of wear rate, friction coefficient, hardness and corrosion resistance [83]

and steady frictional value and was calculated by the Motosh's equation as given by

$$\mu = \frac{\cos \beta \left(\frac{T_{input}}{F_{opposing}} - \frac{P}{2\pi} \right)}{r_t + r_n \cos \beta} \quad (13)$$

Using the above equation, torque angle slope were apprehended during the make-up procedure that employed to characterize the functioning of applied coating. The results obtained by the experiments illustrated that non-cyanide Ag-PTFE coating was depicting low magnitude of the friction coefficient and make-up torque than the five times thicker cyanide based coating.

Then scientists tried to implicate MoS₂ and graphite in the matrix of PTFE to improve the tribological characteristics of the sliding surfaces [99, 108–110]. Although it has improved the tribological properties of the surfaces by reducing the friction and increasing the wear resistance but the presence of the MoS₂ imparts spontaneous coalesce of inorganic particle, as a consequence there was unstable frictional coefficient and hence the durability of the applied surface coating reduced [111, 112].

In recent year, researchers had made-up with a new and advanced coating method of "a nano-copper based composite coating (AFRICO)" that was the mixture of nano-copper suspension incorporating with PTFE particles and acrylic resin as a binder [91]. The AFRICO coatings resulted

Table 6 Experimental observations of augmenting PTFE concentration on friction coefficient, hardness, wear rate and corrosion resistance [83]

Concentration of PTFE	Friction coefficient (μ)	Hardness (Hv)	Wear rate (mm ³ /Nm)	Corrosion current density (A/dm ²)	Tafel plot (V/decade)	
					Anodic (β_a)	Cathodic (β_c)
Only deposited Ni-P	0.32	506	6.48×10^{-6}	3.75×10^{-3}	0.162	-0.148
deposited 14.4 vol% of PTFE + Ni/P	0.16	325	4.88×10^{-6}	1.52×10^{-6}	0.131	-0.135
deposited 27.4 vol% of PTFE + Ni/P	0.13	323	5.33×10^{-6}	1.21×10^{-6}	0.098	-0.114

in decreased in the frictional value owing to the low frictional characteristics of PTFE [86, 87] and the nano-copper particles present in the matrix acts as a ball bearing within the contact surface [93]. Meng et al. [91] and Zhao [113] illustrated numerous galling test at varying make-up torque from 5790 to 13150 N on phosphate treated AFRICO surface as shown in Fig. 10 and they observed that the AFRICO based coatings were superior than the solitary phosphate coating as these coating resulted in 20% drop in the make-up torque from 8800 to 6600 Nm. The role of the phosphating layer is to prevent the cracking and spalling of the applied coat.

They also reported that these coating depicted high resistance towards the corrosion caused in the environment containing supersaturated Carbon dioxide (CO₂) and Hydrogen sulfide (H₂S) gasses.

3.2 FEP (fluorinated ethylene propylene)

The foremost TFE copolymer was Fluorinated ethylene propylene (FEP), which was accidentally produced by copolymerization of TFE and hexafluoropropylene (HFP). FEP was commercially commenced in the market during 1960 by DuPont. The framework of FEP is like PTFE excluding that a trifluoromethyl group was adapted along to main framework as depicted in Fig. 11. Basically, FEP is formed by the copolymerization of TFE and HFP in an aqueous medium with a free radical initiator and a dispersing agent. The

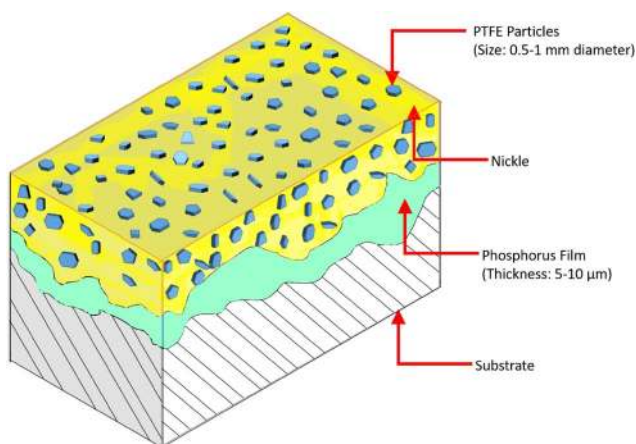


Fig. 10 Applied Ni-P/PTFE coating on substrate

Fig. 11 Polymerization of FEP



Co-monomer ratio and the polymerizing circumstances are prudently controlled in order to attain the desired Copolymer composition and molecular weight, which are in close relation to with melt viscosity, processability and the mechanical properties of the final products [79, 114].

FEP not only possesses tribological properties similar to PTFE, but also it owns higher hardness, lower molecular weight, and easy machining. Hence owing to these comprehensive characteristics, it is substituting PTFE in many tribological applications [115, 116]. Zhizhong Feng et al. [117] investigated the tribological properties of FEP coating through conventional flame spraying technique. Initially, the substrate was sand-blasted and cleaned in an ultrasonic bath of ethanol. Following to cleaning, the substrate was thermally sprayed with the FEP powder of particle size of about 100 μm along with acetylene as fuel gas at 0.05–0.08 Mpa of pressure. They characterized the thermally sprayed coating of FEP under wear-test under dry- and water-lubricated conditions and reported the significant drop in frictional coefficient from 0.36 to 0.17.

Also, many researchers had scrutinized the synergistic effects of FEP with other fluoropolymers that resulted in a further decrease in wear rate. Zang et al. [118] had studied the tribological and hydrophobic behaviors of phenolic coatings reinforced with FEP powder of 15 μm in diameter. During the frictional test, they observed the considerable lower frictional value of around 0.14. Similarly, the addition of FEP in the PTFE coating had also resulted in a decrease in the friction coefficient and hence improved the wear life of the system. It was due to the fact that the FEP has a lower viscosity than PTFE at the melting state, as a consequence less heat is generated, leading to lower temperatures. Thus, during the sliding of PTFE/FEP composites, the FEP adhere better than the PTFE on the polishing scratches resulting in the decrease in wear rate owing to the lubricating action of FEP incorporated on the counterface [119].

3.3 Poly[tetrafluoroethylene-co-(perfluoroalkyl vinyl ether)] or perfluoroalkoxy polymer (PFA)

After the introduction of FEP, further research on TFE copolymers led to the development of PFA (Fig. 12)—a copolymer of TFE and perfluoropropylvinylether (PPVE) in 1972 by DuPont. The commercial PFA products are Teflon

PFA from DuPont, Aflon PFA from Asahi Glass, Dyneon PFA from Dyneon, Neoflon PFA from Daikin, and Hyflon PFA from Solvay [79, 80].

Commonly, PFA is prepared by an aqueous dispersion process. Lower relative molecular mass amplifies the melt flow rate of PFA while keeping the high operating temperature, chemical permanency, and lower frictional performance of PTFE. The adding of PAVE co-monomer to the TFE backbone expressively decreases the crystallinity of PFA compared to PTFE comprising identical relative molecular mass. The compact crystallinity is critical in order to improve the fatigue fracture resistant of fluoro-polymers [80, 120]. However PFA has comparable mechanical, thermal and chemical characteristics as PTFE, owing to this PFA has rarely been considered in tribological applications. The deficiency of tribology application of PFA composites is also due to the augmented cost as a comparison to PTFE [121–123]. Sidebottom et al. [121] studied wear and frictional performance of PFA coating over PTFE coating. The preliminary frictional coefficient (average over initial 1000 cycles) for virgin PFA was 0.29 and it gradually decreased over time to a concluding value of 0.24. This was expressively higher than the value of unfilled PTFE ($\mu \sim 0.14$). The reason for this difference in friction has been assigned to the perfluoroethoxy (C_2F_5O -) side groups in PFA disrupting the smooth molecular profile of the linear fluoropolymer.

Mateus et al. [121] also tried to analyze the wear resistant characteristics of thermal sprayed ceramic ($Al_2O_3-TiO_2$)-polymer PFA and PTFE composite coating on an aluminum substrate. During ball and disc test, ceramic($Al_2O_3-TiO_2$)—8 vol% PFA showed much lower friction coefficient of 0.2 than that of ceramic ($Al_2O_3-TiO_2$)—8 vol% PTFE composite coating. The reason behind this was the loss of PTFE during thermal spraying PTFE/ceramic coating. This observation can be recognized to its high viscosity at the melting situation than the PFA that averts it from flowing by the substrate surface, which results in lesser adhesion than the PFA particles. Correspondingly, researchers had also tried to incorporate PFA with multiwalled carbon nanotubes (MWNTs). The better compatibility of PFA i.e. simultaneously it can serve the purpose of binder and adhesives, it gives high carbon yield when the pyrolyzing and self-lubricious property of composite had resulted in a decrease in the value of friction coefficient and improved wear resistance.

3.4 Polyether ether ketone (PEEK)

Polyether ether ketone (PEEK) is a colorless organic thermoplastic polymer in the polyaryletherketone (PAEK) line. It was formerly familiarized by Victrex PLC, now Imperial Chemical Industries (ICI) in beginning of the 1980s. The step-growth PEEK polymers are obtained by step-growth polymerizing of dialkylation of bisphenolate salts as depicted in Fig. 13 [124]. PEEK is a kind of engineering plastic with outstanding performance: High mechanical properties (strength, modulus, toughness, Resistance to creep, abrasion and fatigue), high temperature resistance ($T_g = 143\text{ }^\circ\text{C}$, $T_m = 338\text{ }^\circ\text{C}$, continuous service temperature of $250\text{ }^\circ\text{C}$, heat distortion temperature often above $300\text{ }^\circ\text{C}$), very low flammability, good resistance to aggressive solvent, favorable processing capability, high wear resistance and self-lubrication, etc. [125–128].

Although PEEK has excellent performance, it still cannot meet the modern industrial machinery- heat and frictional performance, therefore PEEK and its composites filled with fibers, inorganic, and organic have become a trend. Commonly used reinforcing materials are as follows: the nanoparticles such as silicon dioxide (SiO_2), ZrO_2 , Si_3N_4 , AlN , and Al_2O_3 ; fibers such as carbon fiber, steel fiber, and PTFE fiber; whiskers such as potassium carbonate whiskers and zinc oxide whiskers; and so on. Henceforth it has applications in aerospace, military, nuclear plants, chemical process equipment, and oil-well applications [129–141].

Bijwe et al. [127] investigated the optimal fraction (up to 30%) of PTFE in PEEK. The conclusions from the experiment exhibited decrease in frictional coefficient and wear rate with increasing proportion of PTFE contents. In a different approach, Vail et al. [142] used high tenacity expanded polytetrafluoroethylene (ePTFE) filaments as both fiber reinforcement and reservoir for solid lubricants in PEEK. The wear rates and friction coefficient obtained from the ePTFE filled composites were better than conventionally filled PTFE-PEEK composites. Sumer et al. [142] investigated the tribological behavior of the PEEK and the glass fiber reinforced PEEK composite under dry sliding and water lubricated conditions, using friction and wear tests as well as an optical microscope for the microstructural characterization. They reported the following findings: In this study, the tribological performance of pure polyetheretherketone (PEEK) and 30 wt% fiber glass (GFR) reinforced PEEK composite were studied at dry sliding and

Fig. 12 Formulation of PFA



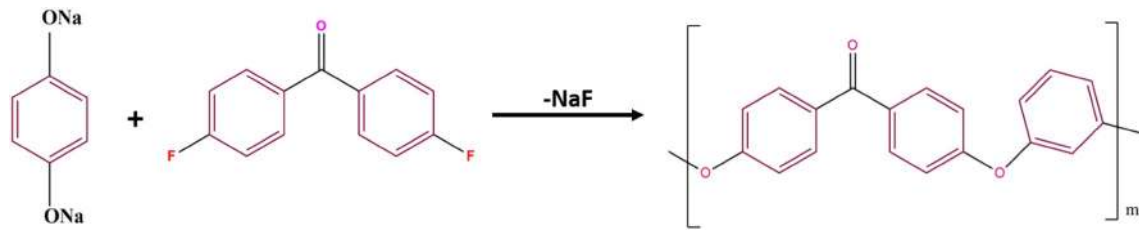


Fig. 13 Preparation of PEEK

water lubricated conditions. Wear evaluation were performed with the configuration of a rotating AISI D2 disc mounted with polymer pin. Test conditions were atmospheric conditions, 1.77, 3.54, 5.30 MPa pressures and 0.80, 1.60 m/s sliding speeds. The results demonstrate that the coefficient of friction and specific wear rates for pure PEEK and PEEK + 30 wt% GFR composite increases slightly with the increase in applied pressure values. Conversely, the coefficient of friction was decreasing while the specific wear increased with the increase in sliding speed values. The influence of GFR fiber on the coefficient of friction and wear of the composite is more pronounced at the dry wear test condition. Finally the specific wear rates for pure PEEK and PEEK + 30 wt% GFR underwater lubricated condition were in the order of 10–15 m²/N while under dry sliding condition this value is in the order of 10–14 m²/N.

Recently, researchers had also tried to incorporate short carbon fibers (SCFs) and graphite in PEEK in order to avert wear and friction. Lin et al. [142] studied the tribological behavior of PEEK/SCF/graphite composite in addition with the filler nanoparticles of ZnS and TiO₂. During sliding, these nanoparticles ZnS/TiO₂ were released into the contact region under severe load conditions, owing to which there was tribosintering of these released particles and resulted in the formation of secondary protective coating. This secondary proactive coating eventually increases the load carrying capacity, reduction in friction coefficient and improved wear resistance of the system.

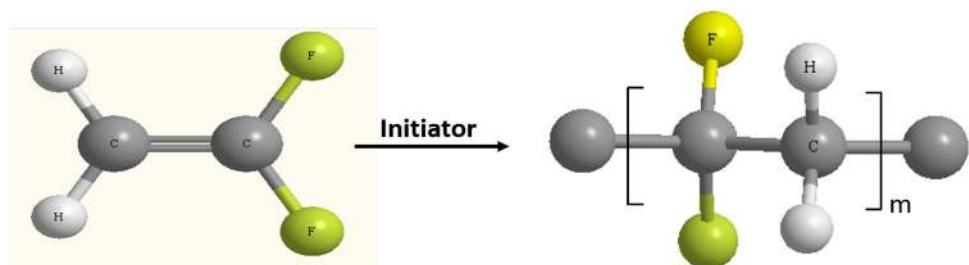
3.5 Polyvinylidene fluoride (PVDF)

Another class of fluoro-based polymers is Polyvinylidene fluoride (PVDF), that was commercially introduced by Pennsalt (now Arkema) with the tradename Hylar[®] PVDF, Kynar[®], Teflon[®] in 1961. PVDF is a partially fluorinated, semi-crystalline polymer, which is a consequence of free-radical co-polymerization of vinylidene fluoride (VDF) as depicted in Fig. 14. PVDF is commonly conceived by two classes of copolymerization approaches, the first is suspension method and another is the emulsion method. Suspension copolymerization yields PVDF with a high head-to-tail structure in the polymer chains, owing to which there is an increase in crystallinity, melting temperature, and better mechanical characterization such as strength, toughness, and wear resistance at elevated temperatures [79]. In accumulation, it also owns excellent anti-radiation properties in contrasted to PTFE, making it a suitable candidate for tribological material [143].

PVDF is a polymer owning numerous crystalline arrangements depending on the processing conditions. The crystallinity of PVDF increases significantly in the first week after processing and stabilizes after 4 weeks. This phenomenon increases crystallinity up to 65% and results in the intrinsic stress and the potential stress cracking [79].

Researchers tried to improve the wear resistance of the PVDF with the addition of carbon nano-fiber, TiO₂, modified nano-CeO₂ (MN-CeO₂), Polyamides (PA), polymethylmethacrylate (PMMA) [144–148]. Brostow et al. [149] studied the influence of varying the amount of carbon black (CB) on the tribology of PVDF/ultrahigh relative

Fig. 14 Preparation of PVDF



molecular mass of polyethylene (UHMWPE) (70/30) composite, wherein an optimized CB amount reduced the wear expressively. Zhu et al. [150] formulated g-C₃N₄/PVDF composites through wet mixing and hot press molding method, and observed that the inclusion of g-C₃N₄ efficiently enhanced the thermal permanency and wear behavior of neat PVDF. Wang et al. [151] scrutinized the tribocorrosion characteristics in association with superhydrophilicity of PVDF when incorporated with FEP and carbon nanofibers (CNFs). Initially, dispersion solution of 1 g PVDF powders, 0.1 g FEP powders and 0.01 g CNFs was prepared in 10 mL absolute alcohol. Afterward, the solution was discharged on the pretreated aluminum plate by means of an air spray gun underneath 6 bar of pressure for 5 min. During characterization, they observed that the 10 wt% FEP showcased the best super-hydrophobicity i.e. water contact angle of 164°, improved wear and corrosion resistance. The reason for such enhancement in the properties was due to augmentation interface adhesive strength of the prepared coating owing to the cross-linking effect of PVDF macromolecules via the formation of C–C or C=C functional groups during the curing process.

3.6 Ethylene chlorotrifluoroethylene (ECTFE) and Ethylene tetrafluoroethylene (ETFE)

The foremost fluoropolymer encompassing ethylene entities was ECTFE, that commercialized via the Italian establishment Ausimont during 1970. ECTFE is a mutable copolymer of ethylene & chlorotrifluoroethylene (CTFE) as presented in Fig. 15a. ECTFE is formulated by the copolymerization of ethylene and CTFE at comparatively

low temperatures i.e. less than 10 °C, inside an aqueous medium by means of a peroxide catalyst & a halogenated solvent chain transfer agent to control the relative molecular mass [152, 153].

ECTFE is a packed and a zigzag arrangement of polymer, owing to that ECTFE has a crystallinity of 50–60%. The melting temperature ECTFE is in the range of 220–245 °C subject to the polymerization approaches and can be utilized over an expansive temperature go from –100 to 150 °C. ECTFE can be prepared by the standard handling techniques for conventional thermoplastics in the scope of 260–300 °C [80, 152, 153].

As the copolymer with ethylene, ECTFE has reasonable chemical resistant, flame resistant, and dielectric constant of around 2.6. While, despite of that it has phenomenal radiation retardation, weathering resistant, and boundary properties, just as great tensile, flexural and wear-related properties. The strength, wear resistant and creep resistant of ECTFE is significantly more noteworthy than of PTFE and FEP. The sole biggest utilization of ECTFE is in fire safety protection and aviation industries, for example, gaskets for fluid oxygen and different fuels, segments for shuttle and airship lodges, tangled tubing, and hoses for space suits. Toward the end of 1999, Ausimont formulated a new family of ECTFE resins under the trademark Vatar, explicitly designed to meet the necessities for fire retardant applications. ECTFE is at present fabricated by Solvay under the trademark Halar in the wake of securing Ausimont in 2002 [79].

Subsequently ECTFE, the supplementary fluoropolymer comprising ethylene units—ETFE was marketed in 1973 by DuPont. ETFE involved substituting ethylene and TFE

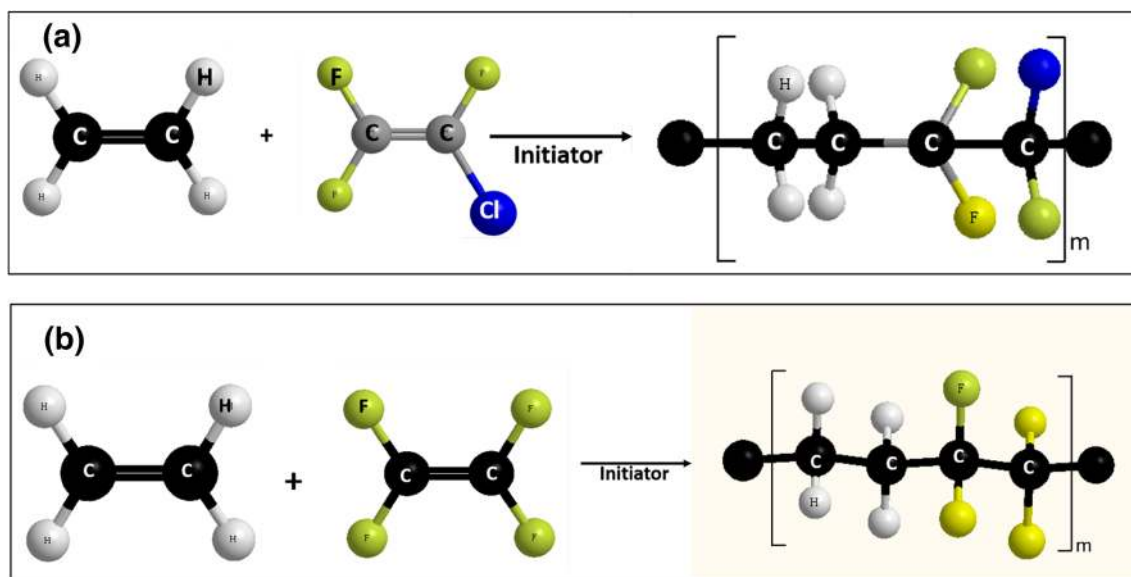


Fig. 15 Preparation of **a** ECTFE, **b** ETFE

units in the polymer principal chain as shown in Fig. 15. The crystallinity of ETFE ranges from 40 to 60%, and it has a melting temperature of 225–300 °C relying upon the comonomer proportion and the processing technique. ETFE has predominant processability and improved mechanical properties contrasted with other TFE copolymers. ETFE can be handled by all preparing techniques, for example, injection molding, compression molding, blow molding, rotational molding, and extrusion [79, 80].

ETFE has higher tensile strength, higher flexibility, better impact strength, reasonable stiffness, better abrasion resistance, and higher cutting resistant. ETFE unified by glass fiber reinforcement is tougher and stiffer and has higher tensile strength than PTFE, PFA or FEP. ETFE has a comprehensive operating temperature range from – 100 to 150 °C. Its radiation resistance is higher with the advantage of being cross-connected by high-energy radiation. The foremost application for ETFE is wire and cable insulation, representing 60% of its market. ETFE has good resistant to petroleum and fuel penetration, brought about a noteworthy development of ETFE as fuel tubing. The business ETFE items incorporate Tefzel[®] from DuPont, Fluon from Asahi Glass, Halon ETFE from Solvay, Neoflon ETFE from Daikin, and Dyneon ETFE from Dyneon [79, 154, 155]. The comprehensive understanding of the above-discussed fluoropolymer has been summarized in Table 7.

4 Limitation of fluoro-based polymers

With the advancement in the field of medical, researchers had tried to mimic the skeleton metabolisms and fabricated artificial implants that are capable of serving the same function and these implants are made-up of

metallic material owing to high tensile strength, toughness, availability at low cost, high durability, and ease of fabrication [90]. The major challenges for them is to sustain their bio-compatibility, bio-safety and bio-functionality in the human body having certain magnitude of pH value. A team investigators during their research perceived that employed artificial-implants such as hip-replacement, dental implants, screws to hold them, spinal implants, and many more failed, owing to corrosion and *in vivo-galling* [158–167]. The anti-galling characteristic of the sliding surface can be improved by various means as discussed in the previous sections out of which the application of the fluoro-based functional coating is the most suitable method that was adopted to counter the issue friction, wear and *in vivo-galling* [168–171]. Although these coatings served the purpose of improved anti-galling properties but the fluorine present in them act as a bio-transformation precursor i.e. it results in the metabolism imbalance in human body and sometime can result in trauma as during austere conditions fluoro-polymers gets degrade and releases hydrofluoric acids [77, 172].

5 Conclusion

In this fast-paced technology, it is still inexorable to manufacture a product without any surface irregularities and their existence results in friction, generation of heat, noise, wear and galling. Galling and wear is the ominous result of friction that is frequently perceived by numerous engineering components where there is juxtaposition and sliding of one surface over other e.g. piston-cylinder arrangement, sheet-metal forming process, couplers, fasteners and even in bio-implants that results in the inter-diffusion of sliding surfaces, seizing

Table 7 The summary of fluoropolymers and their properties [79–82, 121, 156, 157]

	PTFE	FEP	PFA	PVDF	ECTFE	ETFE
Starting year	1947	1960	1972	1961	1970	1973
Specific gravity	2.1–2.3	2.13–2.15	2.12–2.17	1.78	1.68	1.71
Melting temperature (°C)	317–337	260–282	302–310	155–192	235–245	254–279
Tensile strength (MPa)	23	14.5–21	28–31	35–50	28–30	38–48
Tensile modulus (Mpa)	550	345	276	1040–2070	240	827
Operating temperature (°C)	– 260 to 260	210 (max.)	260 (max.)	– 20 to 30	– 100 to 150	– 100 to 150
Frictional coefficient (μ)	0.05–0.2	0.12–0.20	0.2–0.3	0.2–0.4	0.2–0.5	0.24–0.5
Break elongation (%)	300–550	300	300	50–250	250–300	150–300
Dielectric strength (kV/mm)	19.7	19.7	19.7	63–67	80	14.6
Thermal conductivity (W/mK)	0.25	0.209	0.21	0.2	0.15	0.238
Crystallinity (%)	92–98	65–75	48	35–70	50–60	40–60
Beginning of absorbed radiation dose (Mrad)	0.02	0.2	0.02	08–16	6–10	20

of components and eventually failure of the system. Though, The application of fluoropolymers such as PTFE, FEP, PFA, ECTFE and ETFE, efficiently reduces wear and friction of the system, but their synergistic effect with carbon nanofibers(CNTs), Ceramics- $\text{Al}_2\text{O}_3/\text{TiO}_2$, modified nano- CeO_2 (MN- CeO_2), Polyamides (PA), polymethylmethacrylate (PMMA) and multiwalled nanocarbon tubes(MWNTs) for significantly averts wear, corrosion and in some cases it also improves the surface hardness and hence concocting them as suitable candidate in various tribocorrosion applications from marine and petroleum industries to defense and space sector. Simultaneously, a swift advancement is needed in the versatility of these fluoropolymers for checking in vivo galling and tribocorrosion and improving bio-compatibility. The fluoro-based polymers have come a long way in the past 8 decades. No doubt many new fluoro-based polymer materials will be developed and new applications will be found for old fluoropolymers, which finally leading the evolution of science and technology to advanced level which can be utilized by all for refining the vitality of the humanoid world.

Acknowledgements The authors would like to thank Dr. CP Ramanarayanan, Vice-Chancellor, DIAT (DU), Pune, for constant encouragement and support. The authors would also like to acknowledge Mr. Prakash Gore, Mr. Swaroop Gharde, Mr. Deepak Prajapati, Mr. Rushikesh Ambekar, Mr. Jay Korde and Ms. Kirti Thakur for technical discussions and support.

Compliance with ethical standards

Conflict of interest The authors declare that they have no conflict of interest.

References

- Semaw S, Rogers MJ, Quade J et al (2003) 2.6-Million-year-old stone tools and associated bones from OGS-6 and OGS-7, Gona, Afar, Ethiopia. *J Hum Evol* 45:169–177. [https://doi.org/10.1016/S0047-2484\(03\)00093-9](https://doi.org/10.1016/S0047-2484(03)00093-9)
- Stapert D, Johansen L (1999) Flint and pyrite: making fire in the stone age. *Antiquity* 73:765–777. <https://doi.org/10.1017/S0003598X00065510>
- Baugh D (1999) The miracle of fire by friction. In: Wescott D (ed) *Primitive technology: a book of earth skills*. Gibbs Smith Publisher, Salt Lake
- Sorensen A, Roebroeks W, Van Gijn A (2014) Fire production in the deep past? The expedient strike-a-light model. *J Archaeol Sci* 42:476–486
- Hough W (1890) Aboriginal fire-making. *Am Anthropol* 3:359–372
- Hutchings I, Shipway P (2017) *Tribology: friction and wear of engineering materials*. Elsevier Science, Amsterdam
- Popov VL (2000) Contact mechanics and friction. In: Childs T, Maekawa K, Obikawa T, Yamane Y (eds) *Metal machining*. Elsevier, Amsterdam, pp 363–374
- Kato K (2011) History of tribology. *Tribol Online* 6:ii. <https://doi.org/10.2474/trol.6.ii>
- Bhushan B (2013) *Introduction to tribology*. Wiley, Hoboken, p 368
- Johnson KL, Kendall K, Roberts AD (1971) Surface energy and the contact of elastic solids. *Proc R Soc A Math Phys Eng Sci* 324:301–313. <https://doi.org/10.1098/rspa.1971.0141>
- Mo Y, Turner KT, Szlufarska I (2009) Friction laws at the nanoscale. *Nature* 457:1116–1119. <https://doi.org/10.1038/nature07748>
- Glaeser W (1971) Friction and wear. *IEEE Trans Parts Hybrids Packag* 7:99–105. <https://doi.org/10.1109/TPHP.1971.1136416>
- Roberts AD, Jackson SA (1975) Sliding friction of rubber. *Nature* 257:118–120. <https://doi.org/10.1038/257118a0>
- Derjaguin BV, Muller VM, Toporov YP (1975) Effect of contact deformations on the adhesion of particles. *J Colloid Interface Sci* 53:314–326. [https://doi.org/10.1016/0021-9797\(75\)90018-1](https://doi.org/10.1016/0021-9797(75)90018-1)
- Blau PJ, Budinski KG (1999) Development and use of ASTM standards for wear testing. *Wear* 225–229:1159–1170. [https://doi.org/10.1016/S0043-1648\(99\)00045-9](https://doi.org/10.1016/S0043-1648(99)00045-9)
- ASTM Standard (1991) G98-91. ASTM, West Conshohocken
- Komanduri R, Shaw MC (1975) Galling wear of materials at high speed sliding contact. *Wear* 33:283–292. [https://doi.org/10.1016/0043-1648\(75\)90283-5](https://doi.org/10.1016/0043-1648(75)90283-5)
- Kontis P, Li Z, Segersäll M et al (2018) The role of oxidized carbides on thermal-mechanical performance of polycrystalline superalloys. *Metall Mater Trans A*. <https://doi.org/10.1007/s11661-018-4709-x>
- Schedin E, Lehtinen B (1993) Galling mechanisms in lubricated systems: a study of sheet metal forming. *Wear* 170:119–130. [https://doi.org/10.1016/0043-1648\(93\)90358-5](https://doi.org/10.1016/0043-1648(93)90358-5)
- Metselaar HSC, Kerkwijk B, Mulder EJ et al (2001) Wear of ceramics due to thermal stress: a thermal severity parameter. *Wear* 249:962–970. [https://doi.org/10.1016/S0043-1648\(01\)00832-8](https://doi.org/10.1016/S0043-1648(01)00832-8)
- Bos J, Moes H (1994) Frictional heating of elliptic contacts. *Tribol Ser* 27:491–500. [https://doi.org/10.1016/S0167-8922\(08\)70334-1](https://doi.org/10.1016/S0167-8922(08)70334-1)
- van der Heide E, Schipper DJ (2003) Galling initiation due to frictional heating. *Wear* 254:1127–1133. [https://doi.org/10.1016/S0043-1648\(03\)00324-7](https://doi.org/10.1016/S0043-1648(03)00324-7)
- Karlsson P (2012) The early stage of galling. Thesis, Karlstads University
- Karlsson P, Krakhmalev P, Gåård A, Bergström J (2013) Influence of work material proof stress and tool steel microstructure on galling initiation and critical contact pressure. *Tribol Int* 60:104–110. <https://doi.org/10.1016/j.triboint.2012.10.023>
- Karlsson P, Gåård A, Krakhmalev P, Bergström J (2012) Galling resistance and wear mechanisms for cold-work tool steels in lubricated sliding against high strength stainless steel sheets. *Wear* 286–287:92–97. <https://doi.org/10.1016/j.wear.2011.04.002>
- Podgornik B, Hogmark S, Sandberg O (2006) Proper coating selection for improved galling performance of forming tool steel. *Wear* 261:15–21. <https://doi.org/10.1016/j.wear.2005.09.005>
- Dong W, Xu L, Lin Q, Wang Z (2017) Experimental and numerical investigation on galling behavior in sheet metal forming process. *Int J Adv Manuf Technol* 88:1101–1109. <https://doi.org/10.1007/s00170-016-8843-6>
- Kalpajian S, Schmid R, Sekar V (2013) *Manufacturing engineering and technology*, 7th edn. Pearson Publications, Singapore

29. Bruschielli L, Latorrata V (2018) The influence of “shell behavior” on load distribution for thin-walled conical joints. *J Appl Mech* 67:298–306
30. Yuan G, Yao Z, Han J, Wang Q (2004) Stress distribution of oil tubing thread connection during make and break process. *Eng Fail Anal* 11:537–545. <https://doi.org/10.1016/j.engfailana.2003.10.007>
31. Rooij M de (1998) Tribological aspects of unlubricated deep-drawing processes. FEBO druk, pp 7–31
32. Zhou L, Gao K, Zheng X et al (2018) Developing of galling during the forming and its improvement by physical vapour depositing. *Surf Eng* 34:493–503. <https://doi.org/10.1080/02670844.2017.1381375>
33. Yangui W, Guermazi N, Elleuch K (2016) Failure analysis of a cold work tool material slides against carbon steel in sheet metal forming process—a case study of hinges production. *Int J Adv Manuf Technol*. <https://doi.org/10.1007/s00170-016-9015-4>
34. Podgornik B, Jerina J (2012) Surface and coatings technology surface topography effect on galling resistance of coated and uncoated tool steel. *Surf Coat Technol* 206:2792–2800. <https://doi.org/10.1016/j.surfcoat.2011.11.041>
35. Aragay G, Pons J, Merkoçi A (2011) Recent trends in macro-, micro-, and nanomaterial-based tools and strategies for heavy-metal detection. *Chem Rev* 111:3433–3458. <https://doi.org/10.1021/cr100383r>
36. Smallman R, Dillamore I, Dobson P et al (1966) The measurement of stacking fault energy to cite this version: HAL Id: jpa-00213120. *Le J Phys Colloq* 27:C3–C86
37. Yadav R, Naebe M, Wang X, Kandasubramanian B (2016) Body armour materials: from steel to contemporary biomimetic systems. *RSC Adv* 6:115145–115174. <https://doi.org/10.1039/c6ra24016j>
38. Korde JM, Shaikh M, Kandasubramanian B (2018) Bionic prototyping of honeycomb patterned polymer composite and its engineering application. *Polym Plast Technol Eng*. <https://doi.org/10.1080/03602559.2018.1434667>
39. Mishra N, Kandasubramanian B (2017) Biomimetic design of artificial materials inspired by iridescent nacre structure and its growth mechanism. *Polym Plast Technol Eng* 2559:1–15. <https://doi.org/10.1080/03602559.2017.1326139>
40. Deoray N, Kandasubramanian B (2018) Review on three-dimensionally emulated fiber-embedded lactic acid polymer composites: opportunities in engineering sector. *Polym Plast Technol Eng* 57:860–874. <https://doi.org/10.1080/03602559.2017.1354226>
41. Yadav R, Naebe M, Wang X, Kandasubramanian B (2017) Review on 3D prototyping of damage tolerant interdigitating brick arrays of Nacre. *Ind Eng Chem Res* 56:10516–10525. <https://doi.org/10.1021/acs.iecr.7b01679>
42. Sahoo BN, Kandasubramanian B (2014) Recent progress in fabrication and characterisation of hierarchical biomimetic superhydrophobic structures. *RSC Adv* 4:22053–22093. <https://doi.org/10.1039/c4ra00506f>
43. Gore PM, Zachariah S, Gupta P, Balasubramanian K (2016) Multifunctional nano-engineered and bio-mimicking smart superhydrophobic reticulated ABS/fumed silica composite thin films with heat-sinking applications. *RSC Adv* 6:105180–105191. <https://doi.org/10.1039/c6ra16781k>
44. Podgornik B, Majdic F, Leskovsek V, Vizintin J (2012) Improving tribological properties of tool steels through combination of deep-cryogenic treatment and plasma nitriding. *Wear* 288:88–93. <https://doi.org/10.1016/j.wear.2011.04.001>
45. Budinski KG (1981) Incipient galling of metals. *Wear* 74:93–105. [https://doi.org/10.1016/0043-1648\(81\)90196-4](https://doi.org/10.1016/0043-1648(81)90196-4)
46. Reed-Hill RE, Abbaschian RAR (2008) Physical metallurgy principles, 4th edn. Cengage Learning, Boston
47. Pearson WB (2013) A handbook of lattice spacings and structures of metals and alloys. International series of monographs on metal physics and physical metallurgy, vol 4. Elsevier Science, Amsterdam
48. Persson DHE, Jacobson S, Hogmark S (2003) The influence of phase transformations and oxidation on the galling resistance and low friction behaviour of a laser processed Co-based alloy. *Wear* 254:1134–1140. [https://doi.org/10.1016/S0043-1648\(03\)00325-9](https://doi.org/10.1016/S0043-1648(03)00325-9)
49. Fourdeux A, Berghezan A, Webb WW (1960) Stacking faults in zinc. *J Appl Phys* 31:918–920. <https://doi.org/10.1063/1.1735718>
50. Wang WY, Shang SL, Wang Y et al (2014) Effects of alloying elements on stacking fault energies and electronic structures of binary Mg alloys: a first-principles study. *Mater Res Lett* 2:29–36. <https://doi.org/10.1080/21663831.2013.858085>
51. Zhao YH, Liao XZ, Horita Z et al (2008) Determining the optimal stacking fault energy for achieving high ductility in ultrafine-grained Cu–Zn alloys. *Mater Sci Eng, A* 493:123–129. <https://doi.org/10.1016/j.msea.2007.11.074>
52. Takeuchi S, Suzuki K, Maeda K, Iwanaga H (1985) Stacking-fault energy of II–VI compounds. *Philos Mag A Phys Condens Matter Struct Defects Mech Prop* 50:171–178. <https://doi.org/10.1080/01418618408244220>
53. Fast L, Ahuja R, Nordström L et al (1997) Anomaly in *c/a* ratio of Zn under pressure. *Phys Rev Lett* 79:2301
54. Callister WD, Rethwisch DG (2007) Materials science and engineering: an introduction. Wiley, New York
55. Bhansali KJ, Miller AE (1982) The role of stacking fault energy on galling and wear behavior. *Wear* 75:241–252. [https://doi.org/10.1016/0043-1648\(82\)90151-X](https://doi.org/10.1016/0043-1648(82)90151-X)
56. Eyre TS, Alsalim H (1977) Effect of boronising on adhesive wear of titanium alloys. *Tribol Int* 10:281–285. [https://doi.org/10.1016/0301-679X\(77\)90208-0](https://doi.org/10.1016/0301-679X(77)90208-0)
57. Davis JR (2001) Surface engineering for corrosion and wear resistance. ASM International, Materials Park
58. Podgornik B, Kafexhiu F, Kosec T et al (2017) Friction and anti-galling properties of hexagonal boron nitride (h-BN) in aluminium forming. *Wear* 388–389:2–8. <https://doi.org/10.1016/j.wear.2017.04.026>
59. Verlinden B (2005) Severe plastic deformation of metals. *Metal Metall* 11:165–182. <https://doi.org/10.30544/380>
60. Clark KP (2017) Pvp 2017–65261 the effects of low temperature carbon diffusion treated fasteners on thread galling resistance. *Proc ASME* 1:1–7. <https://doi.org/10.1115/PVP201765261>
61. Hu PS, Liu R, Liu J, McRae G (2014) Investigation of wear and corrosion of a high-carbon stellite alloy for hip implants. *J Mater Eng Perform* 23:1223–1230. <https://doi.org/10.1007/s11665-014-0887-x>
62. Sivakumar B, Pathak LC, Singh R (2017) Role of surface roughness on corrosion and fretting corrosion behaviour of commercially pure titanium in Ringer’s solution for bio-implant application. *Appl Surf Sci* 401:385–398. <https://doi.org/10.1016/j.apsusc.2017.01.033>
63. Daure JL, Carrington MJ, Shipway PH et al (2018) A comparison of the galling wear behaviour of PVD Cr and electroplated hard Cr thin films. *Surf Coat Technol* 350:40–47. <https://doi.org/10.1016/j.surfcoat.2018.06.070>
64. Dong Y, Zheng K, Fernandez J et al (2018) Tribology and hot forming performance of self-lubricious NC/NiBN and NC/WC: C hybrid composite coatings for hot forming die. *J Mater Process Technol* 252:183–190. <https://doi.org/10.1016/j.jmatp.rotec.2017.09.025>

65. Miyoshi K, Sanders JH, Hager CH et al (2008) Wear behavior of low-cost, lightweight TiC/Ti-6Al-4V composite under fretting: effectiveness of solid-film lubricant counterparts. *Tribol Int* 41:24–33. <https://doi.org/10.1016/j.triboint.2007.04.006>
66. Podgornik B, Hogmark S (2006) Surface modification to improve friction and galling properties of forming tools. *J Mater Process Technol* 174:334–341. <https://doi.org/10.1016/j.jmatprotec.2006.01.016>
67. Menezes PL, Reeves CJ, Rohatgi PK, Lovell MR (2013) Self-lubricating behavior of graphite-reinforced composites. In: Menezes PL, Nosonovsky M, Ingole SP, Kailas SV, Lovell MR (eds) *Tribology for scientists and engineers*. Springer, New York, pp 341–389
68. Tu CJ, Chen D, Chen ZH, Xia JT (2008) Improving the tribological behavior of Graphite/Cu matrix self-lubricating composite contact strip by electroplating Zn on graphite. *Tribol Lett* 31:91–98. <https://doi.org/10.1007/s11249-008-9341-2>
69. Cao Y, Du L, Huang C et al (2011) Wear behavior of sintered hexagonal boron nitride under atmosphere and water vapor ambiances. *Appl Surf Sci* 257:10195–10200. <https://doi.org/10.1016/j.apsusc.2011.07.018>
70. Panjan P, Drnovšek A, Kovač J (2018) Tribological aspects related to the morphology of PVD hard coatings. *Surf Coat Technol* 343:138–147. <https://doi.org/10.1016/j.surfcoat.2017.09.084>
71. Fluoropolymers market by type and application—2022. <https://www.alliedmarketresearch.com/fluoropolymers-market>. Accessed 15 Oct 2018
72. Plunkett RJ (1941) Tetrafluoroethylene polymers. US, US2230654
73. Ameduri B, Boutevin B (2004) *Well-architected fluoropolymers: synthesis, properties and applications*. Elsevier, Amsterdam
74. Scheirs J (1997) *Modern fluoropolymers: high performance polymers for diverse applications*. Wiley, New York
75. Jackson HL (1972) *Fluoropolymers*, LA Wall, Ed., Wiley-Interscience, a Division of John Wiley and Sons, Inc., New York, 1972. 550 pp. \$9.95. *J Polym Sci Part B Polym Lett* 10:316
76. Agar S, Baysak E, Hizal G et al (2018) An emerging post-polymerization modification technique: the promise of thiol-para-fluoro click reaction. *J Polym Sci, Part A: Polym Chem* 56:1181–1198. <https://doi.org/10.1002/pola.29004>
77. Henry BJ, Carlin JP, Hammerschmidt JA et al (2018) A critical review of the application of polymer of low concern and regulatory criteria to fluoropolymers. *Integr Environ Assess Manag* 14:316–334. <https://doi.org/10.1002/ieam.4035>
78. Dhanumalayan E, Joshi GM (2018) Performance properties and applications of polytetrafluoroethylene (PTFE)—a review. *Adv Compos Hybrid Mater* 1:247–268. <https://doi.org/10.1007/s42114-018-0023-8>
79. Teng H (2012) Overview of the development of the fluoropolymer industry. *Appl Sci* 2:496–512
80. Ebnasajjad S (2017) Introduction to fluoropolymers. In: Kutz M (ed) *Applied plastics engineering handbook*. Elsevier, Amsterdam, pp 55–71
81. Mateus C, Costil S, Bolot R, Coddet C (2005) Ceramic/fluoropolymer composite coatings by thermal spraying—a modification of surface properties. *Surf Coat Technol* 191:108–118
82. Berry KL (1951) *Aqueous colloidal dispersions of polymers*. US, US2559752
83. Sheu HH, Jian SY, Lin MH et al (2017) Electroless Ni-P/PTFE self-lubricating composite thin films applied for medium-carbon steel substrate. *Int J Electrochem Sci* 12:5464–5482. <https://doi.org/10.20964/2017.06.30>
84. Brown RP (1988) *Plastics materials*. Elsevier, Amsterdam
85. Demas NG, Polycarpou AA (2008) Tribological performance of PTFE-based coatings for air-conditioning compressors. *Surf Coat Technol* 203:307–316. <https://doi.org/10.1016/j.surfcoat.2008.09.001>
86. Ballester E, Sui M, Spokesman CF-N (2000) Effect of PTFE particle size on wear and coefficient of friction. *Natl Lubr Grease Inst* 65:12–17
87. Prajapati AK, Omrani E, Menezes PL, Rohatgi PK (2018) Fundamentals of solid lubricants. In: Menezes P, Rohatgi P, Omrani E (eds) *Self-lubricating composites*. Springer, Berlin
88. Hu Z, Li H, Fu Q et al (2006) Research progress on low friction coefficient solid lubricating coatings. *J Mater Eng* 3:60–68
89. Tulsi SS (1983) Electroless nickel-PTFE composite coatings. *Trans IMF* 61:147–149. <https://doi.org/10.1080/0020967.1983.11870654>
90. Shaffer SJ (2008) Wear and friction testing of hard and soft lubricious coatings in dry sliding for use in small arms action components. *J ASTM Int* 5:1–10
91. Meng Z, Zhang XF, Zhang J et al (2017) Application study of nano-copper based composite anti-friction coating for corrosion resistant couplings. *J Pet Sci Eng* 157:1143–1147. <https://doi.org/10.1016/j.petrol.2017.07.074>
92. Zhao S, Zhang X, Yang D et al (2016) Galling resistance of an anti-friction coating on oil-casing couplings. In: *MATEC web of conferences*. EDP Sciences, p 4017
93. Meng Z, Li Y, Yang Y et al (2015) Effect of a nanoparticulate anti-friction coating on galling resistance of threaded oil-casing couplings. *J Pet Sci Eng* 128:140–144. <https://doi.org/10.1016/j.petrol.2015.02.008>
94. Baragetti PhD S (2002) Effects of taper variation on conical threaded connections load distribution. *J Mech Des* 124:320–329. <https://doi.org/10.1115/1.1456459>
95. Guangjie Y, Zhenqiang Y, Qinghua W, Zhentong T (2006) Numerical and experimental distribution of temperature and stress fields in API round threaded connection. *Eng Fail Anal* 13:1275–1284. <https://doi.org/10.1016/j.engfailana.2005.11.006>
96. Tester S, Karpat F (2016) Experimental studies on galling onset in OCTG connections: a review 1. *Energy Resour Technol ASME* 130:1–4. <https://doi.org/10.1115/1.2835616>
97. Assanelli AP, Xu Q, Benedetto F et al (1997) Numerical/experimental analysis of an API 8-round connection. *J Energy Resour Technol* 119:3–10. <https://doi.org/10.1115/1.2794980>
98. Ertas A, Carper HJ, Blackstone WR (1992) Development of a test machine and method for galling studies. *Exp Mech* 32:340–347. <https://doi.org/10.1007/BF02325587>
99. Cuvalci O, Sofuoglu H, Ertas A (2003) Effect of surface coating and tin plating on friction characteristics of P-110 tubing for different thread compounds. *Tribol Int* 36:757–764. [https://doi.org/10.1016/S0301-679X\(03\)00057-4](https://doi.org/10.1016/S0301-679X(03)00057-4)
100. Srinivasan KN, John S (2005) Studies on electroless nickel—PTFE composite coatings. *Surf Eng* 21:156–160. <https://doi.org/10.1179/174329405X40902>
101. Arora R, Singh N, Balasubramanian K, Alegaonkar P (2014) Electroless nickel coated nano-clay for electrolytic removal of Hg ions. *RSC Adv* 4:50614–50623. <https://doi.org/10.1039/C4RA06988A>
102. Yadav R, Balasubramanian K (2015) Metallization of electrospun PAN nanofibers via electroless gold plating. *RSC Adv* 5:24990–24996. <https://doi.org/10.1039/C5RA03531G>
103. Khanale M, Balasubramanian K (2016) Molecular simulation of geometrically optimized polyoxymethylene/poly (vinylalcohol) gel membrane for electroless scrubbing Ni(II) ions. *J Environ Chem Eng* 4:434–439. <https://doi.org/10.1016/j.jece.2015.11.044>

104. Kaleicheva JK, Karaguiozova Z (2018) Improvement of the wear resistance of ferrous alloys by electroless plating of nickel. *IOP Conf Ser Mater Sci Eng* 295:012036. <https://doi.org/10.1088/1757-899X/295/1/012036>
105. Zhao Q, Liu Y, Liu G (2002) Graded Ni–P–PTFE coatings and their potential applications. *Surf Coat Technol* 155:279–284
106. Sieh R, Le HR, Cree AM (2015) Process optimisation of non-cyanide Ag–PTFE metal matrix composite electroplating for threaded connections. *Trans IMF Int J Surf Eng Coatings* 93:232–240. <https://doi.org/10.1080/00202967.2015.1114723>
107. Sieh R, Le H (2018) Evaluation of environmental friendly Ag–PTFE composite coating for use in threaded compression fittings. *Proc Inst Mech Eng Part J J Eng Tribol* 232:503–512. <https://doi.org/10.1177/1350650117719775>
108. Zhang H-J, Zhang Z, Guo F (2011) Studies of the influence of graphite and MoS₂ on the tribological behaviors of hybrid PTFE/Nomex fabric composite. *Tribol Trans* 54:417–423. <https://doi.org/10.1080/10402004.2011.553027>
109. Uthaman N, Majeed A, Pandurangan (2006) Impact modification of polyoxymethylene (POM). *E-Polymers*. <https://doi.org/10.1515/epoly.2006.6.1.438>
110. Pernice G, Corporation W (2015) The evolution and application development of high-performance. In: *Offshore technology conference*, pp 1–4
111. Mohammad A (2015) Tribology of engineering and coated materials in the presence of environmentally friendly refrigerant, pp 123–125
112. Hou X, He J, Yu L et al (2014) Applied surface science preparation and tribological properties of fluorosilane surface-modified lanthanum trifluoride nanoparticles as additive of fluoro silicone oil. *Appl Surf Sci* 316:515–523. <https://doi.org/10.1016/j.apsusc.2014.07.171>
113. Sun L-H, Yang Z-G, Li X-H (2008) Mechanical and tribological properties of polyoxymethylene modified with nanoparticles and solid lubricants. *Polym Eng Sci* 48:1824–1832. <https://doi.org/10.1002/pen.21150>
114. Gangal SV, Brothers PD (2010) Perfluorinated polymers, perfluorinated ethylene–propylene copolymers. *Encycl Polym Sci Technol* 4–9
115. Wang Q, Wang Y, Wang H et al (2016) Experimental investigation on tribological behavior of several polymer materials under reciprocating sliding and fretting wear conditions. *Tribol Int* 104:73–82. <https://doi.org/10.1016/j.triboint.2016.08.030>
116. Yan F-Y, Xue Q-J (1998) Study of fretting wear behaviors of FEP. *J Appl Polym Sci* 67:1119–1125. [https://doi.org/10.1002/\(SICI\)1097-4628\(19980207\)67:6%3c1119:AID-APP20%3e3.0.CO;2-U](https://doi.org/10.1002/(SICI)1097-4628(19980207)67:6%3c1119:AID-APP20%3e3.0.CO;2-U)
117. Feng Z, Xu H, Yan F (2008) Preparation of flame sprayed poly(tetrafluoroethylene-co-hexafluoropropylene) coatings and their tribological properties under water lubrication. *Appl Surf Sci* 255:2408–2413. <https://doi.org/10.1016/j.apsusc.2008.07.110>
118. Song H-J, Zhang Z-Z (2006) Study on the tribological and hydrophobic behaviors of phenolic coatings reinforced with PFW, PTFE and FEP. *Surf Coat Technol* 201:1037–1044. <https://doi.org/10.1016/j.surfcoat.2006.01.014>
119. Moon-Hee H, Su-Il P (1991) Effect of fluorinated ethylene propylene copolymer on the wear behaviour of polytetrafluoroethylene. *Wear* 143:87–97. [https://doi.org/10.1016/0043-1648\(91\)90087-B](https://doi.org/10.1016/0043-1648(91)90087-B)
120. Sidebottom MA, Junk CP, Salerno HLS et al (2018) Wear-induced microstructural and chemical changes in poly [tetrafluoroethylene-co-(perfluoroalkyl vinyl ether)] (PFA). *Macromolecules* 51:9700–9709
121. Sidebottom MA, Pitenis AA, Junk CP et al (2016) Ultralow wear perfluoroalkoxy (PFA) and alumina composites. *Wear* 362:179–185
122. Crosby JM, Theberge JE, Talley KL (1981) Melt processible fluoropolymer composites. *J Elastomers Plast* 13:149–155
123. Bowers RC, Zisman WA (1974) Frictional properties of tetrafluoroethylene-perfluoro (propyl vinyl ether) copolymers. *Ind Eng Chem Prod Res Dev* 13:115–118
124. Parker D, Bussink J, van de Grampel HT et al (2012) Polymers, high-temperature. In: Ross J (ed) *Ullmann's encyclopedia of industrial chemistry*. American Cancer Society, New York
125. Harsha AP, Tewari US (2002) Tribo performance of polyaryletherketone composites. *Polym Test* 21:697–709
126. Pan G, Guo Q, Zhang W, Tian A (2009) Fretting wear behaviors of nanometer Al₂O₃ and SiO₂ reinforced PEEK composites. *Wear* 266:1208–1215
127. Bijwe J, Sen S, Ghosh A (2005) Influence of PTFE content in PEEK–PTFE blends on mechanical properties and tribo-performance in various wear modes. *Wear* 258:1536–1542
128. Bahadur S, Gong D (1992) The role of copper compounds as fillers in the transfer and wear behavior of polyetheretherketone. *Wear* 154:151–165
129. Kuo MC, Huang JC, Chen M (2006) Non-isothermal crystallization kinetic behavior of alumina nanoparticle filled poly (ether ether ketone). *Mater Chem Phys* 99:258–268
130. Sattari M, Molazemhosseini A, Naimi-Jamal MR, Khavandi A (2014) Nonisothermal crystallization behavior and mechanical properties of PEEK/SCF/nano-SiO₂ composites. *Mater Chem Phys* 147:942–953
131. Khan MU, Reddy KR, Snguanwongchai T et al (2016) Polymer brush synthesis on surface modified carbon nanotubes via in situ emulsion polymerization. *Colloid Polym Sci* 294:1599–1610
132. Cakici M, Kakarla RR, Alonso-Marroquin F (2017) Advanced electrochemical energy storage supercapacitors based on the flexible carbon fiber fabric-coated with uniform coral-like MnO₂ structured electrodes. *Chem Eng J* 309:151–158
133. Hou X, Hu Y, Hu X, Jiang D (2017) Poly (ether ether ketone) composites reinforced by graphene oxide and silicon dioxide nanoparticles: mechanical properties and sliding wear behavior. *High Perform Polym*. <https://doi.org/10.1177/0954008317701549>
134. Unnikrishnan L, Mohanty S, Nayak SK (2013) Proton exchange membranes from sulfonated poly (ether ether ketone) reinforced with silica nanoparticles. *High Perform Polym* 25:854–867
135. Zhang Z, Breidt C, Chang L, Friedrich K (2004) Wear of PEEK composites related to their mechanical performances. *Tribol Int* 37:271–277
136. Gupta V, Mathur RB, Dhami TL, Bahl OP (2002) Carbon/Kevlar/PEEK thermoplastic composites. *High Perform Polym* 14:285–292
137. Werner P, Altstädt V, Jaskulka R et al (2004) Tribological behaviour of carbon-nanofibre-reinforced poly (ether ether ketone). *Wear* 257:1006–1014
138. Rae PJ, Brown EN, Orler EB (2007) The mechanical properties of poly (ether-ether-ketone) (PEEK) with emphasis on the large compressive strain response. *Polymer (Guildf)* 48:598–615
139. Banerjee S, Kar KK (2016) Aluminum-substituted phosphotungstic acid/sulfonated poly ether ether ketone nanocomposite membrane with reduced leaching and improved proton conductivity. *High Perform Polym* 28:1043–1058
140. Zhang G, Schlarb AK (2009) Correlation of the tribological behaviors with the mechanical properties of poly-ether-etherketones (PEEKs) with different molecular weights and their fiber filled composites. *Wear* 266:337–344

141. Reddy KR, Sin BC, Yoo CH et al (2009) Coating of multiwalled carbon nanotubes with polymer nanospheres through microemulsion polymerization. *J Colloid Interface Sci* 340:160–165
142. Vail JR, Krick BA, Marchman KR, Sawyer WG (2011) Polytetrafluoroethylene (PTFE) fiber reinforced polyetheretherketone (PEEK) composites. *Wear* 270:737–741
143. Min C, Liu D, Shen C et al (2017) Remarkable improvement of the wear resistance of poly (vinylidene difluoride) by incorporating polyimide powder and carbon nanofibers. *Appl Phys A*. <https://doi.org/10.1007/s00339-017-1251-4>
144. Li J, Li XZ (2010) Evaluation of the tribological properties of carbon fiber reinforced poly (vinylidene fluoride) composites. *J Mater Eng Perform* 19:1025–1030
145. Wang H, Mu B, Ren J et al (2009) Mechanical and tribological behaviors of PA66/PVDF blends filled with calcium sulphate whiskers. *Polym Compos* 30:1326–1332
146. Nie WZ, Li J, Li XZ (2010) The addition of carbon fiber on the tribological properties of poly (vinylidene fluoride) composites. *Fibers Polym* 11:559–564
147. Garcia JL, Koelling KW, Seghi RR (1998) Mechanical and wear properties of polymethylmethacrylate and polyvinylidene fluoride blends. *Polymer (Guildf)* 39:1559–1567
148. Jian L, Chilan C (2010) The preparation and tribological properties of PVDF/TiO₂ nanocomposites. *Polym Plast Technol Eng* 49:643–647
149. Brostow W, Keselman M, Mironi-Harpaz I et al (2005) Effects of carbon black on tribology of blends of poly (vinylidene fluoride) with irradiated and non-irradiated ultrahigh molecular weight polyethylene. *Polymer (Guildf)* 46:5058–5064
150. Zhu L, Wang Y, Hu F, Song H (2015) Structural and friction characteristics of g-C₃N₄/PVDF composites. *Appl Surf Sci* 345:349–354
151. Wang H, Liu Z, Wang E et al (2015) A robust superhydrophobic PVDF composite coating with wear/corrosion-resistance properties. *Appl Surf Sci* 332:518–524
152. Moggi G, Bonardelli P, Bart JCJ (1984) Copolymers of 1,1-difluoroethene with tetrafluoroethene, chlorotrifluoroethene, and bromotrifluoroethene. *J Polym Sci Polym Phys Ed* 22:357–365
153. Goldbach JT, Amin-Sanayei R, He W et al (2016) Commercial synthesis and applications of poly (vinylidene fluoride). In: Ameduri B, Sawada H (eds) *Fluorinated polymers: applications, vol 2*. The Royal Society of Chemistry, Science Park
154. Ford TA, Edward HW (1948) Polyvinylidene fluoride and process for obtaining the same. US, US2435537
155. Carlson DP, Kerbow DL, Leck TJ, Olson AH (1986) Heat stable tetrafluoroethylene-perfluoro (alkyl vinyl ether) copolymers. US, US 4599386
156. McCrum NG (1959) An internal friction study of polytetrafluoroethylene. *J Polym Sci* 34:355–369
157. Starkweather HW Jr, Ferguson RC, Chase DB, Minor JM (1985) Infrared spectra of amorphous and crystalline poly (tetrafluoroethylene). *Macromolecules* 18:1684–1686
158. Ayers R, Miller M, Schowinsky J et al (2018) Three cases of metallosis associated with spine instrumentation. *J Mater Sci Mater Med* 29:3. <https://doi.org/10.1007/s10856-017-6011-7>
159. Hall DJ, Urban RM, Pourzal R et al (2017) Nanoscale surface modification by anodic oxidation increased bone ingrowth and reduced fibrous tissue in the porous coating of titanium-alloy femoral hip arthroplasty implants. *J Biomed Mater Res Part B Appl Biomater* 105:283–290. <https://doi.org/10.1002/jbm.b.33554>
160. Fontenot MG, Kent JN (1992) In vitro wear performance of proplast TMJ disc implants. *J Oral Maxillofac Surg* 50:133–139. [https://doi.org/10.1016/0278-2391\(92\)90358-7](https://doi.org/10.1016/0278-2391(92)90358-7)
161. Rogers D (1992) Engineering a device for installing dental implants—ProQuest. *Mech Eng* 114:72–73
162. Vadiraj A, Kamaraj M (2010) Fretting fatigue behavior of surface modified biomedical titanium alloys. *Trans Indian Inst Met* 63:217–223. <https://doi.org/10.1007/s12666-010-0030-0>
163. (2005) Keyword index. *Cell Tissue Bank* 6:315. <https://doi.org/10.1007/s10561-005-4615-5>
164. Gonzalez JEG, Mirza-Rosca JC (1999) Study of the corrosion behavior of titanium and some of its alloys for biomedical and dental implant applications. *J Electroanal Chem* 471:109–115. [https://doi.org/10.1016/S0022-0728\(99\)00260-0](https://doi.org/10.1016/S0022-0728(99)00260-0)
165. Jacobs JJ, Gilbert JL, Urban RM (1998) Corrosion of metal orthopaedic implants. *JBJS* 80:268–282
166. Drevet R, Zhukova Y, Malikova P et al (2018) Martensitic transformations and mechanical and corrosion properties of Fe–Mn–Si alloys for biodegradable medical implants. *Metall Mater Trans A* 49:1006–1013
167. Saikko V (2015) Adverse condition testing with hip simulators. *Biotribology* 1–2:2–10. <https://doi.org/10.1016/j.biotri.2015.02.001>
168. Williams DF (2008) On the mechanisms of biocompatibility. *Biomaterials* 29:2941–2953
169. Li J, Taylor M, Zhang Z (2017) Anti-fouling medical coatings. In: Zhang Z, Wagner VE (eds) *Antimicrobial coatings and modifications on medical devices*. Springer, Berlin, pp 189–214
170. Yi W, Sun Y, Wei X et al (2010) Proteomic profiling of human bone marrow mesenchymal stem cells under shear stress. *Mol Cell Biochem* 341:9–16
171. Nganbe M, Louati H, Khan U et al (2010) Retrieval analysis and in vitro assessment of strength, durability, and distraction of a modular total hip replacement. *J Biomed Mater Res, Part A* 95:819–827
172. Dahlstrom DL, Bloomhuff AB (2014) ACGIH® (American conference of governmental industrial hygienists), pp 178–179

Publisher's Note Springer Nature remains neutral with regard to jurisdictional claims in published maps and institutional affiliations.